PNAS
www.pnas.org

Supplementary Information for

Opposite regulation of Wnt/β-catenin and Shh signaling pathways by Rack1 controls mammalian cerebellar development

Haihong Yang[1#], Qian Zhu[1#], Juanxian Cheng[1], Yan Wu[1], Ming Fan[1,3], Jiyan Zhang[2*], Haitao Wu[1,3*]

*Correspondent authors:
Haitao Wu
E-mail: wuht@bmi.ac.cn

Jiyan Zhang
E-mail: zhangjy@nic.bmi.ac.cn

www.pnas.org/cgi/doi/10.1073/pnas.1813244116

Supplementary Information Text

Results

The overall expression pattern of Rack1 in the developing cerebellum

Previous work has shown that Rack1 is ubiquitously expressed in most adult brain regions, with relatively high levels in hippocampus, olfactory bulb, cortex and cerebellum (1). Here, our immunofluorescence studies further demonstrated that at P3, Rack1 is predominantly expressed in GNPs distributed in the external granular layer (EGL). By P14, Rack1 becomes ubiquitously expressed throughout the cerebellar cortex including EGL, ML, PCL and IGL (Fig. S1A). The expression of Rack1 at both mRNA transcript and protein levels in the cerebellum at the indicated developmental stages suggest Rack1 is highly expressed during the early postnatal stage and gradually decreased thereafter. A similar decrease in the level of Pax6, a GNP marker, during postnatal development was observed (Fig. S1B-D).

Generation of *hGFAP-Cre;Rack1$^{F/F}$* cKO mice

The *hGFAP-Cre* line has been shown to give rise to both neuronal and glial cells that contain the Cre recombinase (2). We first confirmed these results using the Ai9 reporter assay (Fig. S2A,B). Immunofluorescence studies showed specific expression of Cre-recombinase activity in granule neurons and Bergmann glial cells (BGs) but not in Purkinje cells (PCs) (Fig. S2B) (3), suggesting a majority of cells in the cerebellum, not including Purkinje cells, had undergone recombination. These mice were intercrossed with *Rack1$^{F/F}$* mice, which carried loxP sites flanking exon 2 of the *Rack1* gene (4). The expression of Rack1 in whole cerebellar lysates was significantly reduced in *hGFAP-Cre;Rack1$^{F/F}$* mice compared to control *Rack1$^{F/F}$* mice (Fig. S2C). Residual Rack1 detected in the lysates may be due to its expression in Purkinje cells, oligodendrocytes and blood vessel in the cerebellum (3).

Generation of *Atoh1-Cre;Rack1$^{F/F}$* cKO mice

Previous studies have demonstrated the bHLH transcription factor Math1/Atoh1 governs the proliferation of GNPs in the rhombic lip region (5, 6). *In vivo*, the *Atoh1-Cre* recombinase is first detected at E12.5 in GNPs, which give rise to mature granule neurons predominantly in rostral lobules. By E17.5, the Cre-recombinase can also be detected in

the caudal lobules (7, 8). We first characterized the expression pattern of *Atoh1-Cre* recombinase in the cerebellum with the Ai9 reporter assay (Fig. S4A,B), and confirmed the specific expression of Cre-recombinase activity in granule neurons (Fig. S4B). Rack1 expression in the cerebellum lysates of *Atoh1-Cre;Rack1$^{F/F}$* mutants was decreased by up to 50% compared to controls (Fig. S4C). The mutant mice also showed reduced body weight and cerebellar size (Fig. S4D-F, P=0.0193, n≥6).

EdU-labeling show proliferation and migration deficits in *Atoh1-Cre;Rack1$^{F/F}$* mice

At P7, the fraction of EdU+ cells in the EGL was significantly reduced in mutant mice compared to that in control mice in rostral areas (24.02±2.08 in KO vs 58.33±2.36 in WT, P=0.0003, n≥4), but not in caudal areas (52.66±1.85 in KO vs 54±2.75 in WT, P=0.6575, n≥4) (Fig. S5A,B). In rostral areas of *Atoh1-Cre;Rack1$^{F/F}$* mutants, similar to *hGFAP-Cre;Rack1$^{F/F}$* mutants, a significantly increased number of BrdU-incorporating cells was retained at the ML in mutants compared with control (2106±279/mm^2 in KO *vs* in 533±83/mm^2 WT, P<0.0001, n=5) (Fig. S5C,D, arrowheads).

BrdU/EdU double-labeling show impaired self-renewal in *hGFAP-Cre;Rack1$^{F/F}$* and *Atoh1-Cre;Rack1$^{F/F}$* mice

Previous studies have applied sequential nucleoside analog labeling to illustrate the proliferation and self-renewal of NSCs and their progeny (9, 10). Using this assay, we found significantly decreased ratios of EdU$^+$BrdU$^-$ cells/EdU$^+$ cells (24.33±4.49% of that in controls) and EdU$^+$BrdU$^+$ cells/BrdU$^+$ cells (47.64±2.44% of that in controls) in the EGL of *hGFAP-Cre;Rack1$^{F/F}$* mutants at P7 (Fig. 6A-D). Moreover, the ratios of EdU$^+$BrdU$^-$ cells/EdU$^+$ cells and EdU$^+$BrdU$^+$ cells/BrdU$^+$ cells (29.33±2.03% and 63.42±2.39% of that in controls respectively) were also significantly decreased in *Atoh1-Cre;Rack1$^{F/F}$* mutants in rostral areas at P7 (Fig. 6E-H), indicating the impaired self-renewal of GNPs in both *hGFAP-Cre;Rack1$^{F/F}$* and *Atoh1-Cre;Rack1$^{F/F}$* mutant mice.

Generation of *GLAST-CreER^{T2};Rack1$^{F/F}$* cKO mice

Tamoxifen-inducible glial cell-specific *GLAST-CreER^{T2}* knockin driver Cre line was used to generate BG-specific *Rack1* knockout mice. The specificity of Cre recombination was confirmed with the Ai9 reporter assay as described in the manuscript (Fig. S7A). Co-labeling tdTomato+ cells for BLBP, a widely used astrocyte marker, was employed to identify BG cells. In agreement with previous reports (11,12), inducible *GLAST-CreER^{T2}*

expression was mosaic for cortical astrocytes, but revealed a very high efficiency (≥95%) of recombination in cerebellar BGs (Fig. S7B). Moreover, Rack1 staining was abolished in BLBP+ BGs (triangle), but not in PCs (arrowheads) within the PCL following tamoxifen treatment (Fig. S7C), suggesting successful cell-specific *Rack1* deletion in BGs.

Rack1 functions non-cell autonomously to regulate BG and PC morphogenesis

Based on the morphological analysis of *GLAST-CreER^{T2};Rack1$^{F/F}$* mutant cerebellum, we demonstrated that loss of Rack1 in BGs did not affect the gross morphology of the cerebellum, and cerebellar size and cytoarchitecture were unaffected at both ages (Fig. S8A-C). The density and morphology of BGs and their radial processes were indistinguishable between *GLAST-CreER^{T2};Rack1$^{F/F}$* mutants and *Rack1$^{F/F}$* controls (Fig. 4A, Fig. S8C and S9A).

Furthermore, we also examined the morphology, lamination, and expression of PCs in various cell type-specific *Rack1* knockouts. In contrast to NSC- and GNP-specific *Rack1* knockout mice (Fig. 1G, 3D; and Fig. S9A), *GLAST-CreER^{T2};Rack1$^{F/F}$* mutant cerebella appeared to have normal morphology and alignment of PCs at P14 (Fig. S9A). In addition, we also examined Calbindin and *Shh* levels, which are predominately expressed in PCs, at both the protein and transcriptional levels in various *Rack1* conditional knockouts. Calbindin and Shh expression levels were higher in *hGFAP-Cre;Rack1$^{F/F}$* and *Atoh1-Cre;Rack1$^{F/F}$* mutants, but not in *GLAST-Cre/ER^{T2};Rack1$^{F/F}$* mutants, compared to *Rack1$^{F/F}$* controls (Fig. S9B-J). Thus, due to the significantly decreased cerebellar volume and size in both *hGFAP-Cre;Rack1$^{F/F}$* and *Atoh1-Cre;Rack1$^{F/F}$* mutants (Fig. 1A-C and 3A-C; Fig. S2E and S4E), the overall number of PCs may not be affected in *Rack1* knockout.

Together, these results (Fig. S2B, S4B, and S7C) suggest that Rack1 functions non-cell autonomously *via* NSCs and GNPs to regulate BGs and PC development.

Rack1 is essential for Shh signaling activation in GNPs

We first confirmed that Rack1 physically interacts with the Shh signaling receptor Smoothened in the developing cerebellum by co-immunoprecipitation (Fig. S10A). Treatment with the Smoothened agonist (SAG, 3μM) in primary GNPs cells significantly enhanced the interaction between Rack1 and Smoothened (Fig. S10B,C), suggesting

Rack1 might serve as a critical scaffolding protein to mediate Smoothened activation and upregulate downstream Gli1 expression (Fig. S10D). To further test this hypothesis, Rack1 loss-of-function assay was carried out *in vitro* by delivery of Cre recombinase-expressing lentivirus (LV-Cre-GFP) in primary *Rack1*$^{F/F}$ GNPs. Ablation of Rack1 in GNPs dramatically diminished the SAG-induced upregulation of Gli1 and HDAC1/HDAC2 observed in control cells (Fig. S10E,F), suggesting SAG-induced activation of downstream Gli1 is Rack1-dependent. Taken together, these data suggest that Rack1 in the GNPs is required for SAG-induced Shh signaling activation.

Ablation of β-catenin in GNPs does not affect Rack1 expression *in vitro*

Previous studies have demonstrated that Wnt/β-catenin signaling plays critical role for cerebellar morphogenesis (11-13). To test whether Wnt/β-catenin signaling could activate the transcription and expression of Rack1 and HDAC1 in GNPs, primary GNPs were isolated from P4 *Ctnnb1*$^{F/F}$ cerebellum and infected with LV-Cre-GFP lentivirus to knock out the *Ctnnb1* gene. Rack1 and HDAC1 expression were indistinguishable between LV-Cre-GFP infected cells and LV-GFP infected control cells (Fig. S11A,B), suggesting β-catenin does not directly control Rack1 and HDAC1 expression in primary GNPs.

Simultaneous deletion of β-catenin in *hGFAP-Cre;Rack1*$^{F/F}$ mutants significantly rescues locomotor defects.

Compared to *Rack1*$^{F/F}$ control mice, *hGFAP-Cre;Rack1*$^{F/F}$ mice at P20 were notably ataxic, showing abnormal walking patterns including significantly decreased stride length (SL), fore-base width (FB) and hind-base width (HB) ($P<0.001$, n=6) (Fig. S13A,B). Notably, all of the above locomotor defects were effectively rescued in *hGFAP-DKO* mice ($P<0.001$, n=6) (Fig. S13B). To further confirm functional locomotor rescue in double knockouts, we next employed an additional behavioral assay, the rotarod test. *hGFAP-Cre;Rack1*$^{F/F}$ mutants spent significantly less time on the accelerating rotarod compared to controls (3.67±0.61 s in KO *vs* 192.00±26.06 s in control, $P<0.001$, n=6), whereas the time on accelerated rotarod was significantly prolonged in *hGFAP-DKO* double mutant mice compared to *hGFAP-Cre;Rack1*$^{F/F}$ mutants (180.00±14.83 s in *hGFAP-DKO vs* 3.67±0.61 s in *hGFAP-Cre;Rack1*$^{F/F}$ *KO*, $P<0.01$, n=6) (Fig. S13C).

Materials and Methods

Genotyping primers

Animals used in this study were genotyped by PCR. PCR primers for *hGFAP-Cre* were GCCTGCATTACCGGTCGATGCAACGA (forward) and GTGGCAGATGGCGCGGCAACACCATT (reverse). Primers for *Atoh1-Cre* were CCGGCAGAGTTTACAGAAGC (forward) and ATGTTTAGCTGGCCCAA ATG (reverse). Primers for *GLAST-CreER*^{T2} were ACAATCTGGCCTGCTACCA AAGC (forward) and CCAGTGAAACAGCATTGCTGTC (reverse). Primers for *Ai9* were GGCATTAAAG CAGCGTATCC (forward) and CTGTTCCTGT ACGGCATGG (reverse). Primers for *Rack1*$^{F/F}$ were CGCTGCGCCTCTGGGATCTCA (forward) and TGGTGTGGC CGACAAATCGCC (reverse). Primers for *Ctnnb1*$^{F/F}$ were AAGGTAGAGTGATGAAAGTTGTT (forward) and CACCATGTCCTCTGTCTATTC (reverse).

Primary antibodies:

Primary antibodies used for immunofluorescent staining were shown as follows: Calbindin (C9848, Sigma, 1:400), NeuN (MAB377, Millipore, 1:400), BLBP (ab32423, Abcam, 1:500), Pax6 (ab5790, Abcam, 1:400), Rack1 (R1905, Sigma, 1:400), Cleaved caspase-3 (D175, CST, 1:400), Ki67 (550609, BD, 1:500), Pax2 (ab79389, Abcam, 1:500), GFAP (G3893, Sigma,1:600).

Primary antibodies used for Western blot and Co-immunoprecipitation were shown as follows: Rack1 (610177, BD, 1:2000), HDAC1 (5356, CST, 1:1000), HDAC2 (5113, CST, 1:1000), HDAC6 (2162, CST, 1:1000), SIRT6 (ab62739, Abcam, 1:1000), Gli1 (SAB270018, Sigma, 1:1000), β-catenin (610154, BD, 1:2000), Active-β-catenin (06-665, Millipore, 1:1000), Phospho-β-catenin Thr41/Ser45 (9565, CST, 1:1000), Phospho-β-catenin Ser33/37/Thr41 (9561 ,CST, 1:1000), β-actin (3700, CST, 1:1000) , β-tubulin (2146, CST, 1:1000), HA (3724, CST, 1:2000), GFP (sc-101525, Santa, 1:3000), Flag (F1804, Sigma, 1:5000).

Tamoxifen administration

The 4-Hydroxytamoxifen (4-OH-TAM) (Sigma-Aldrich, H7904) was dissolved in a sunflower seed oil/castor oil mixture (4:1) (Sigma-Aldrich, 8001-21-6; 68187-76-8) at 20 mg/ml. To induce recombination, *GLAST-CreER*^{T2}*;Rack1*$^{F/F}$ mice were intraperitoneally

injected with 50 mg/kg 4-OH-TAM/Oil every day for a total of four injections from E17.5 to P0.

Primary culture of GNPs and lentivirus infection

These techniques were performed as previously described (14). Briefly, cerebella from P7 mice were isolated on ice and the meninges removed. The cerebella were cut and incubated in 0.25% trypsin at 37°C and 5% CO_2 for 30 minutes, and subsequently centrifuged at 1000 rpm for 5 minutes. The supernatant was discarded and the granule neuron inoculation solution added to collect GNPs. The mixture was pipetted onto a 70 μm cell strainer and the filtrate collected and gently added to the Percoll separation solution along the tube wall. The mixture was centrifuged at 400 g for 20 minutes, and he middle layer of white granular cells was gently aspirated into a new centrifuge tube and treated with inoculation solution. The mixture was then centrifuged at 1000 rpm for 5 minutes and the supernatant discarded. The resulting cell pellet was gently resuspended in 10% FBS/HBS and plated onto poly-D-lysine coated wells. After 24 hours, the cell culture solution was replaced with serum-free medium (Neurobasal Medium supplemented with 2% B27, 1% N-2, 1% GlutaMAX, Gibco, 21103-049). The purity of granule neurons and GNPs was more than 85%.

For lentiviral infection, primary GNPs were isolated and cultured from the P7 *Rack1*$^{F/F}$ cerebellum. HBLV-Cre-GFP and HBLV-GFP control lentivirus (Titer: 3×10^8 TU/mL, Hanbio Biotechnology Co., Shanghai) were used to infect primary cultured GNPs at DIV1 at 1×10^6 TU/mL. Infected cells were harvested and lysed in lysis buffer at DIV8 for further experimental assay.

Nissl Staining

Slices mounted on gelatin-coated slides were washed 10 minutes with 0.5% PBS-T for 3 times and then immersed into 0.5% tar-violet solution for 20 minutes. The slices were then quickly rinsed in distilled water and differentiated in 95% ethanol for 2 minutes. They were then dehydrated in 75% ethanol twice, 3 minutes each. Finally, the slices were sealed with neutral resin.

Cell culture and transfection

HEK293T cells and *Daoy* cells were cultured in DMEM (Gibco, C11995500BT) supplemnted with 10% FBS (Gibco, 10091148) medium, 1% glutamine and 1%

Penicillin-Streptomycin (Gibco, 15140-122) at 37°C and 5% CO_2. The following plasmids were generously provided by other laboratories: *Flag-HDAC1*, *Flag-HDAC2*, *HA-MDM2* (Dr. Huiyan Li, National Center of Biomedical Analysis, Beijing, China); *Flag-Rack1*, *Rack1-GFP*; *HA-Ubiquitin* (Dr. Jiyan Zhang, Beijing Institute of Basic Medical Sciences). Cells were treated with SAG (3 μM; MedChemExpress, HY-12848) for 2 days, or MG132 (10 μM; MedChemExpress, A2585) for 8 hours. Lipofectamine 2000 (Thermo, 11668019) was used for transfection following the manufacturer's protocol.

RT–PCR and quantitative PCR

RNA was extracted by Tripure (Roche, 11667165001) from whole cerebella as previously described(15) and cDNA was synthesized using the Synthesis Kit (Roche, 04897030001). Real-time PCR was conducted in triplicates employing Roche SYBR Green PCR master mix with the appropriate forward and reverse primers (see Table S1). For analysis of gene expression changes, we averaged results from three replicates in three independent experiments. Values were normalized to *GAPDH* levels.

Detection of self-renewal ability of granule neuron precursors

P6 mice were given a single intraperitoneal injection of 50 mg/kg 5-bromo-2'-deoxyuridine (BrdU)(Roche, 10280879001). After 23 hours they were intraperitoneally injected with 10 mg/kg of 5-ethynyl-2'-deoxyuridine (EdU)(Sigma-Aldrich, 900584), and sacrificed 1 hour later. BrdU/EdU co-localization staining was performed as described above. The ratio of $EdU^+/BrdU^-$ to EdU^+ cells was counted to evaluate the self-renewal capacity of granule neuron precursor within 1 hour.

Intracerebroventricular (ICV) injection

This technique was performed as previously described (16). P0 mice received an intracerebroventricular injection of romidepsin (MedChemExpress, HY-15149), the specific inhibitor of HDAC1/HDAC2, at 0.6 mg/kg and sacrificed 2 days later for analysis. Briefly, a glass electrode containing the romidepsin solution was gently inserted into the brain at the 1/3 line connection near the middle of the brain between the sagittal suture and the eyes until it reached the lateral ventricle. The romidepsin solution was then gently blown into the ventricle using microliter syringe (Hamilton, 700 series).

Behavioral tests

Accelerating Rotarod: After familiarizing with the experimental apparatus, P20 old mice from distinct genotypes were tested every eight hours for six consecutive trials. In each trial, the speed was accelerated from 4 rpm to 40 rpm over a 5 minute period and the deadline was 300 seconds.

Footprint assay: Non-toxic red and black ink were applied to each mouse's forelimbs and hindlimbs, respectively. The mice walked along a runway with white paper into an enclosed rectangular box (50 cm × 6 cm × 9 cm), leaving their footprints on paper. Stride length (SL), hind-base width (HB) and fore-base width (FB) were measured to characterize the walking pattern.

Figures

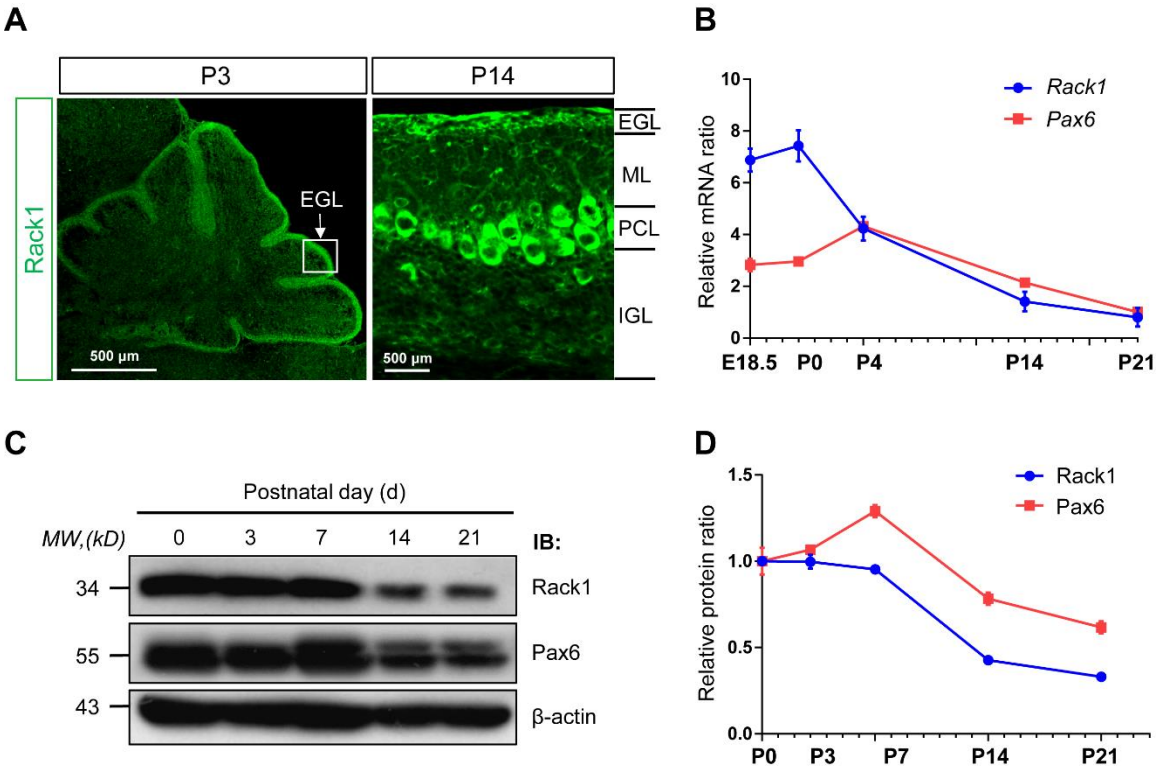

Fig. S1. Expression of Rack1 in the postnatal mouse cerebellum. (A) Immunofluorescent staining with anti-Rack1 shows the distribution of Rack1 in sagittal sections of the mouse cerebellum at P3 and P14, respectively. Scale bar=500 μm. EGL, external granular layer; ML, molecular layer; PCL, Purkinje cell layer; IGL, internal granular layer. (B) The relative *Rack1* and *Pax6* mRNA expression levels in the cerebellum at indicated embryonic and postnatal stages. (C,D) Representative Western blot and relative protein levels of Rack1 and Pax6 in the cerebellum at indicated postnatal days. Mean±SEM, n=4.

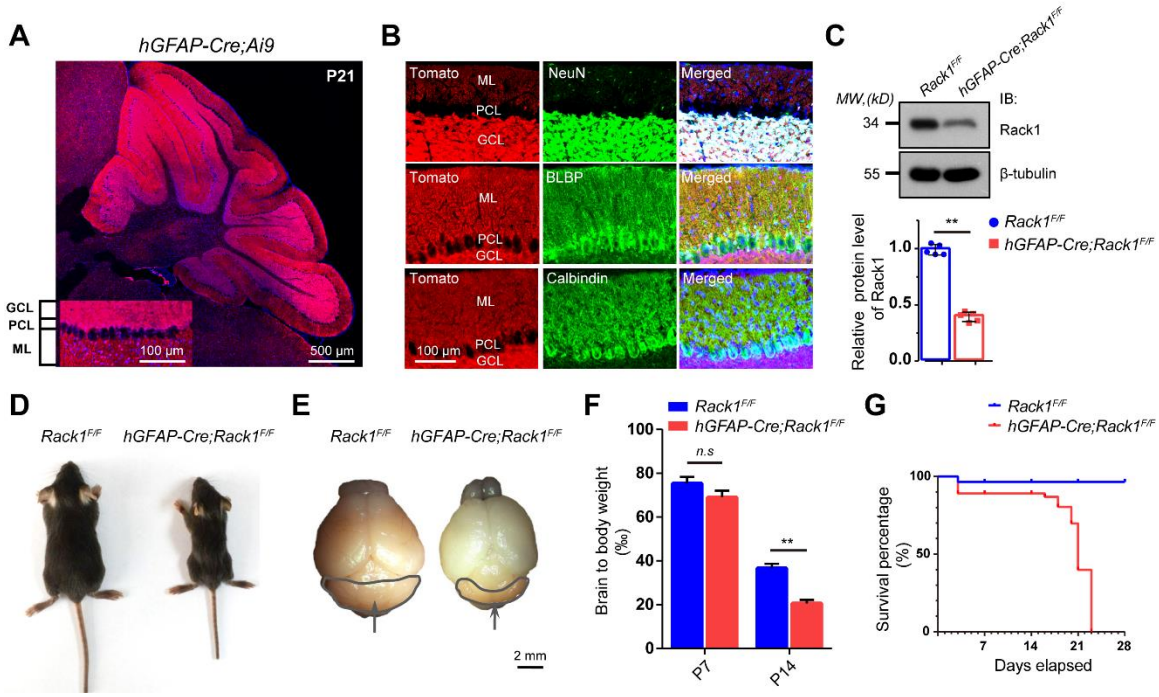

Fig. S2. Generation of NSC-specific *Rack1* conditional mutant mice. (A) *hGFAP-Cre* activity in the cerebellum was analyzed by Rosa26-floxed stop tdTomato (*Ai9*) reporter assay at P21. Scale bar=500 μm; 100 μm. (B) Immunofluorescent staining with anti-NeuN, anti-BLBP and anti-Calbindin shows the co-localization of Tomato fluorescence (Ai9) with NeuN and BLBP, but not with Calbindin. Scale bar=100 μm (C) Representative Western blot and quantification of Rack1 protein level in the control and *hGFAP-Cre;Rack1*$^{F/F}$ mutant cerebellum. Mean±SEM; **P=0.0009, n=5. (D-F) *hGFAP-Cre;Rack1*$^{F/F}$ mutant mice show smaller body size, lack of sulcus and fissure on the surface of cerebellar vermis, and decreased brain to body weight ratio compared to control mice. Mean±SEM; P=0.063 and **P=0.004, respectively, n=3. (G) Survival curves of control and *hGFAP-Cre;Rack1*$^{F/F}$ mutant mice. n=29 for control and n=17 for mutants.

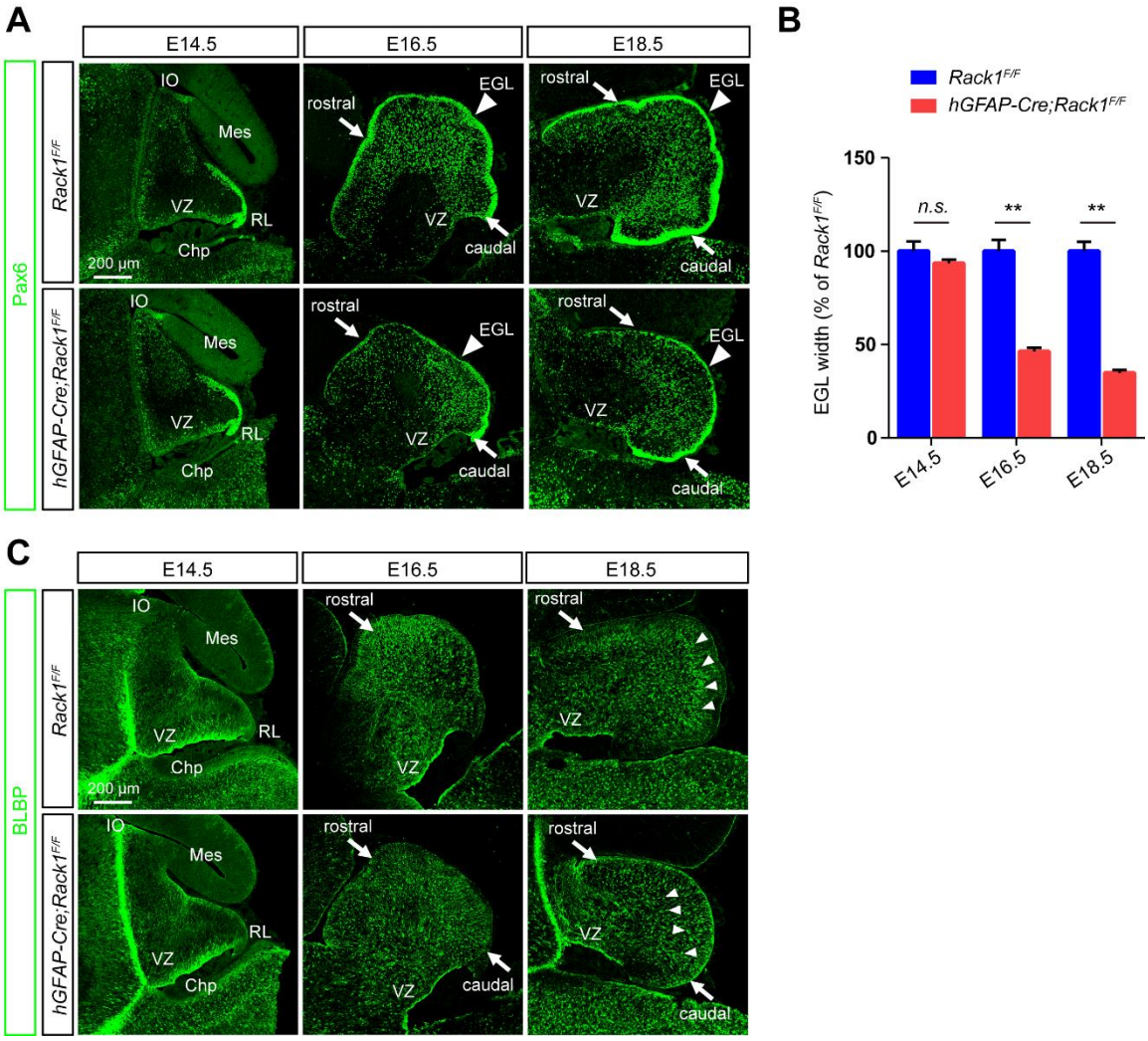

Fig. S3. Embryonic cerebellar developmental abnormalities in *hGFAP-Cre;Rack1$^{F/F}$* mutant mice. (A) Immunofluorescent staining of sagittal sections anti-Pax6 labeled NSCs and GNPs in control and *hGFAP-Cre;Rack1$^{F/F}$* mutant mice at the indicated embryonic stages. Arrowheads point to the EGL region. Scale bar=200 μm. (B) Quantification of EGL width in *hGFAP-Cre;Rack1$^{F/F}$* mutants and *Rack1$^{F/F}$* control mice at the indicated embryonic stages. Mean±SEM; P=0.2993, **P=0.0002, and **P<0.0001, respectively, n=4. (C) Immunofluorescent staining of sagittal sections anti-BLBP labeled radial glial cells and BG precursors at the indicated embryonic stages. Arrowheads point to misaligned BG precursors at E18.5. IO, Isthmic organizer; Mes, mesencephalon; Chp, Choroid plexus; RL, Rhombic lip; VZ, Ventricular zone. Scale bar=200 μm.

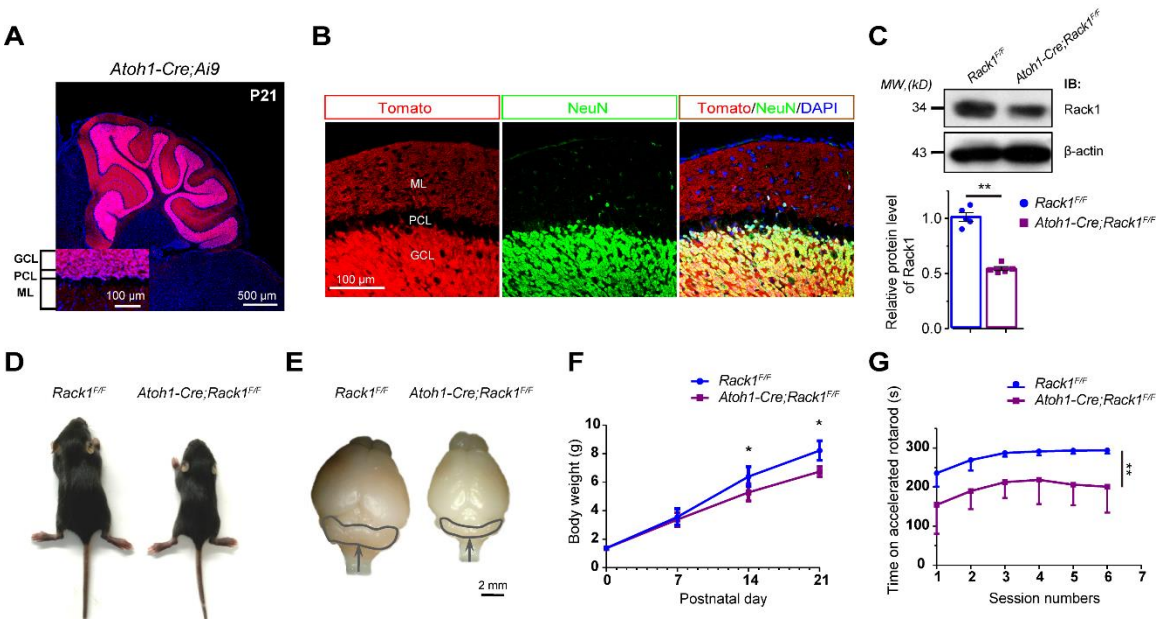

Fig. S4. Generation of GNP-specific *Rack1* conditional mutant mice. (A) *Atoh1-Cre* activity in the cerebellum was analyzed by Rosa26-floxed stop tdTomato (*Ai9*) reporter assay at P21. Scale bar=500 μm; 100 μm. (B) Immunofluorescent staining with anti-NeuN shows Tomato fluorescence (Ai9) co-localized with NeuN. Scale bar=100 μm (C) Representative Western blot and quantification of Rack1 protein level in $Rack1^{F/F}$ control and $Atoh1\text{-}Cre;Rack1^{F/F}$ mutant cerebellum. Mean±SEM; **P=0.0006, n=5. (D-F) $Atoh1\text{-}Cre;Rack1^{F/F}$ mutant mice show smaller body size, lack of sulcus and fissure on the surface of cerebellar vermis, and significantly decreased body weight from P14 to P21. Mean±SEM; *P=0.022 and 0.0193, respectively, n≥6. Scale bar= 2 mm (G) Time spent on the accelerating rotarod in $Rack1^{F/F}$ control and $Atoh1\text{-}Cre;Rack1^{F/F}$ mutant mice. Mean±SEM; **P=0.0275, n≥6.

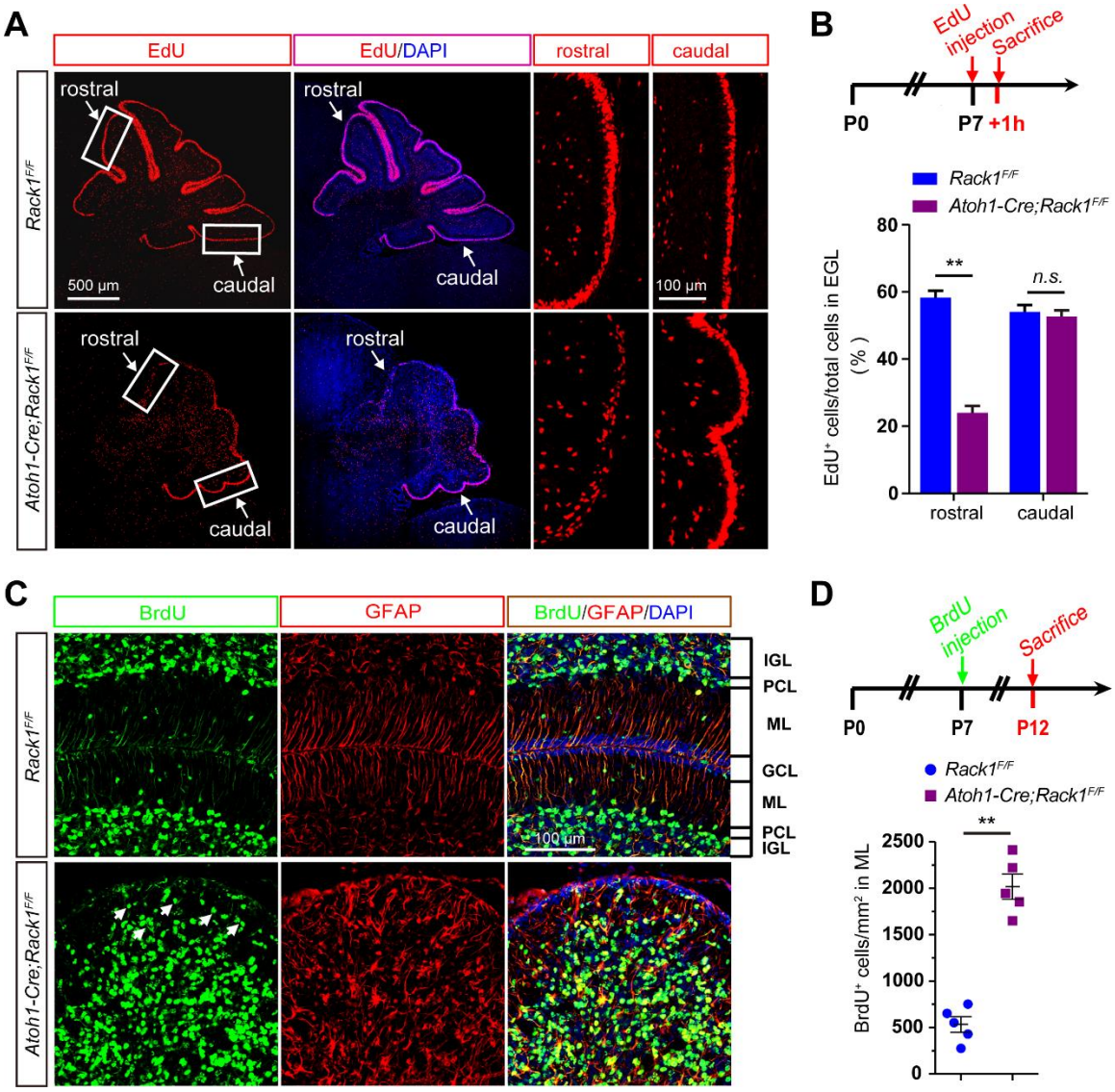

Fig. S5. Ablation of Rack1 disrupts the proliferation and migration of GNPs. (A,B) GNPs proliferation was studied by labeling cells in the S-phase of the cell cycle with EdU in control and *Atoh1-Cre;Rack1*$^{F/F}$ mutant mice at P7 and sacrificed 1h later. Dividing EdU+ cells at P7 were immunofluorescently stained and quantitatively analyzed. Scale bar=500 μm. Arrows indicate the rostral and caudal regions of the cerebellum, respectively. Boxed areas are shown at higher magnification (right) to illustrate rostral-specific decrease in EdU+ cell number in the EGL. Scale bar=100 μm. Mean±SEM; **P=0.0003 and 0.6575, respectively, n=3. (C,D) GNPs migration was studied by immunofluorescent staining to trace BrdU+ cells after a single BrdU pulse at P7 and sacrifice at P12. Anti-GFAP labeled BG radial fiber extensions. Arrows indicate

significantly delayed migrating BrdU+ GNPs in the disrupted ML in *Atoh1-Cre;Rack1*$^{F/F}$ mutant mice. Mean±SEM; **P<0.0001, n=5. Scale bar=100 μm.

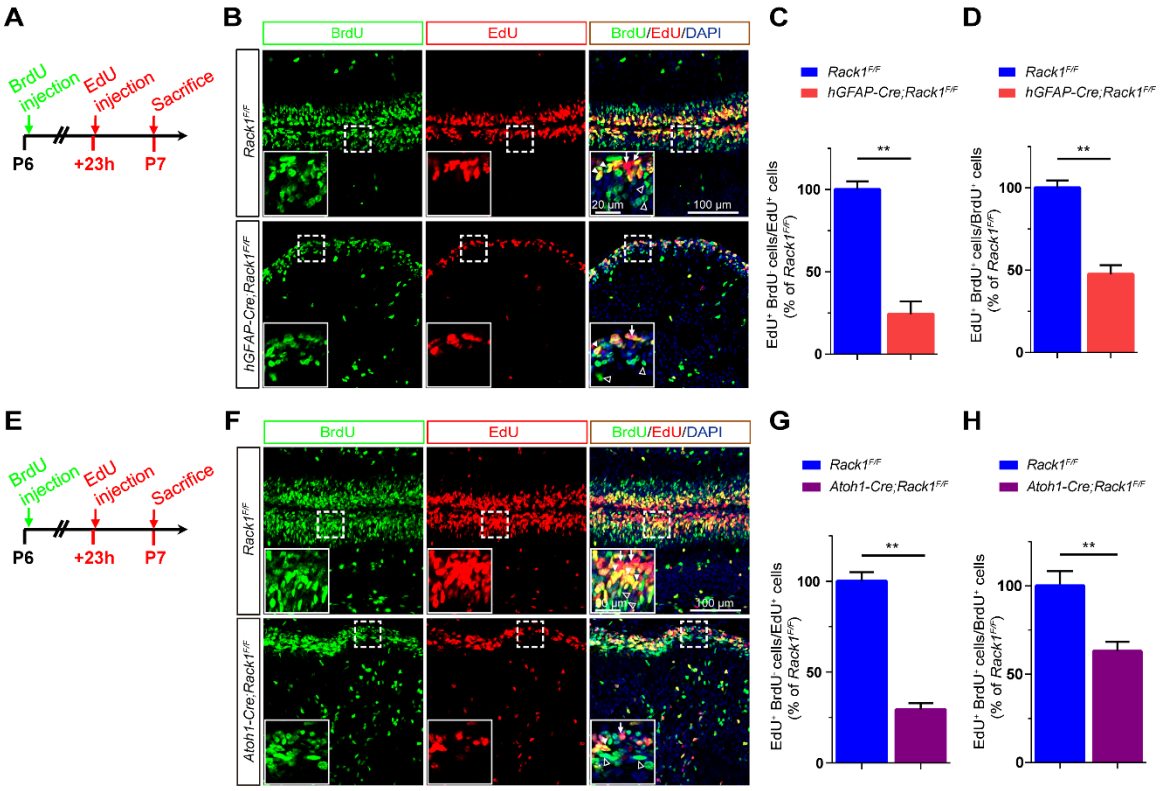

Fig. S6. *Rack1* deletion disrupts GNP self-renewal. (A,B) GNP self-renewal was assessed by sequential BrdU and EdU pulses with an interval of 23 hours at P6 in control and *hGFAP-Cre;Rack1*$^{F/F}$ mice. In the mutant EGL, immunostaining of BrdU (green) and EdU (red) show reduced uridine-incorporated cells compared with controls. Scale bar=100 μm. Areas within the dashed line boxes are shown at higher magnification (bottom left corner) to illustrate cells remaining in cell cycle (EdU^+BrdU^-, indicated with arrows; $BrdU^+EdU^+$, indicated with arrowheads) or cells that have exited the cell cycle ($BrdU^+EdU^-$, indicated with white triangles). Scale bar=20 μm. (C,D) Dividing GNPs were quantitated using the ratio of EdU^+BrdU^- cells to the total number of EdU^+ cells, or the ratio of EdU^+BrdU^+ cells to the total number of $BrdU^+$ cells within the EGL, respectively. A lower percentage of dividing GNPs was detected in *hGFAP-Cre;Rack1*$^{F/F}$ mice than in controls. Mean±SEM; **P=0.0001 and 0.0014, respectively, n=5. (E,F) GNP self-renewal was assessed in control and *Atoh1-Cre;Rack1*$^{F/F}$ mice with the same BrdU/EdU double pulse protocol described above. Scale bars=100 μm; 20 μm. (G,H) Dividing GNPs were quantitated using the ratio of EdU^+BrdU^- cells to the total number

of EdU^+ cells and the ratio of EdU^+BrdU^+ cells to the total number of $BrdU^+$ cells within the EGL as described above. Mean±SEM; **P=0.0018 and 0.0076, respectively, n=5.

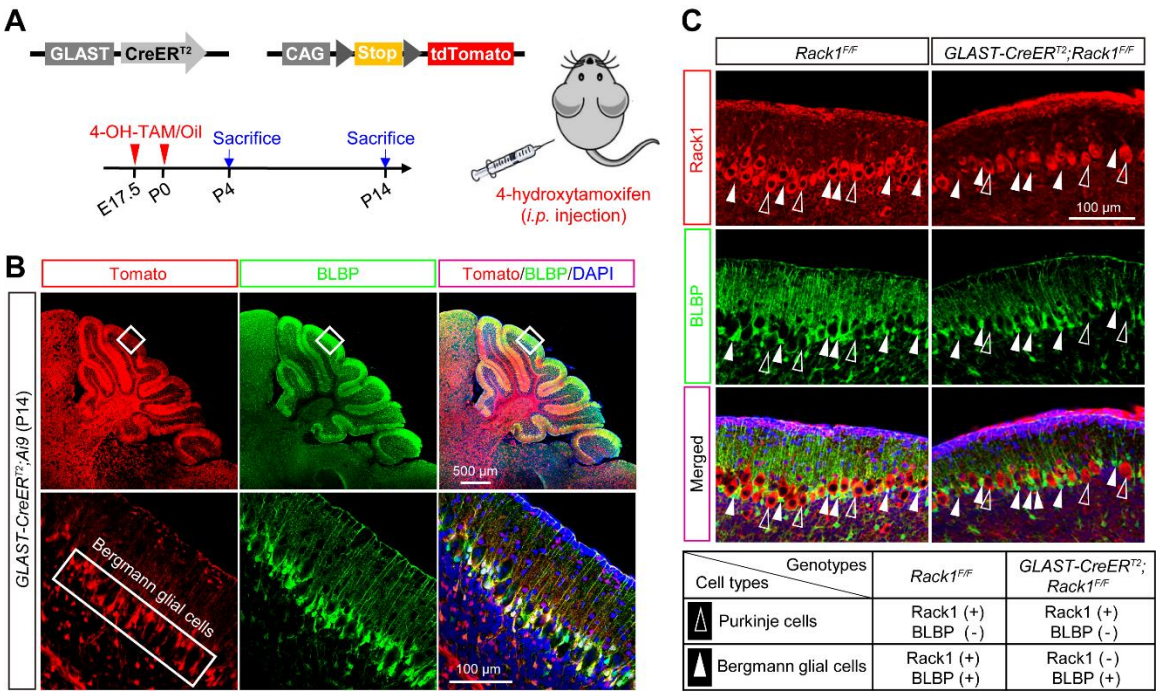

Fig. S7. Generation of BG-specific tamoxinfen-inducible *Rack1* conditional mutant mice. (A) A schematic diagram showing the experimental design to generate *GLAST-CreER^{T2};Rack1$^{F/F}$* mice. 4-OH-TAM was administered 4 times from E17.5 to P0 and sacrificed at either P4 or P14, respectively. (B) Immunofluorescent staining of *GLAST-CreER^{T2}; Ai9* reporter cerebellar section with anti-BLBP illustrates *GLAST-CreER^{T2}*-recombinase activity in BGs. Boxed areas of the cerebellar cortex are shown at higher magnification (bottom) to indicate the co-localization of Tomato+ cells with BLBP+ BGs in the PCL. Scale bar=500 μm; 100 μm. (C) Immunofluorescent staining of cerebellar sections in control and *GLAST-CreER^{T2};Rack1$^{F/F}$* mutants with anti-Rack1 and anti-BLBP, respectively. Rack1^{+}BLBP^{-} PCs are indicated with white triangles, BLBP^{+} BGs are indicated with arrowheads. Table shows that BLBP^{+}Rack1^{+} BGs are present in controls but BLBP^{+}Rack1^{-} BGs in *GLAST-CreER^{T2};Rack1$^{F/F}$* mutants. Scale bar=100 μm.

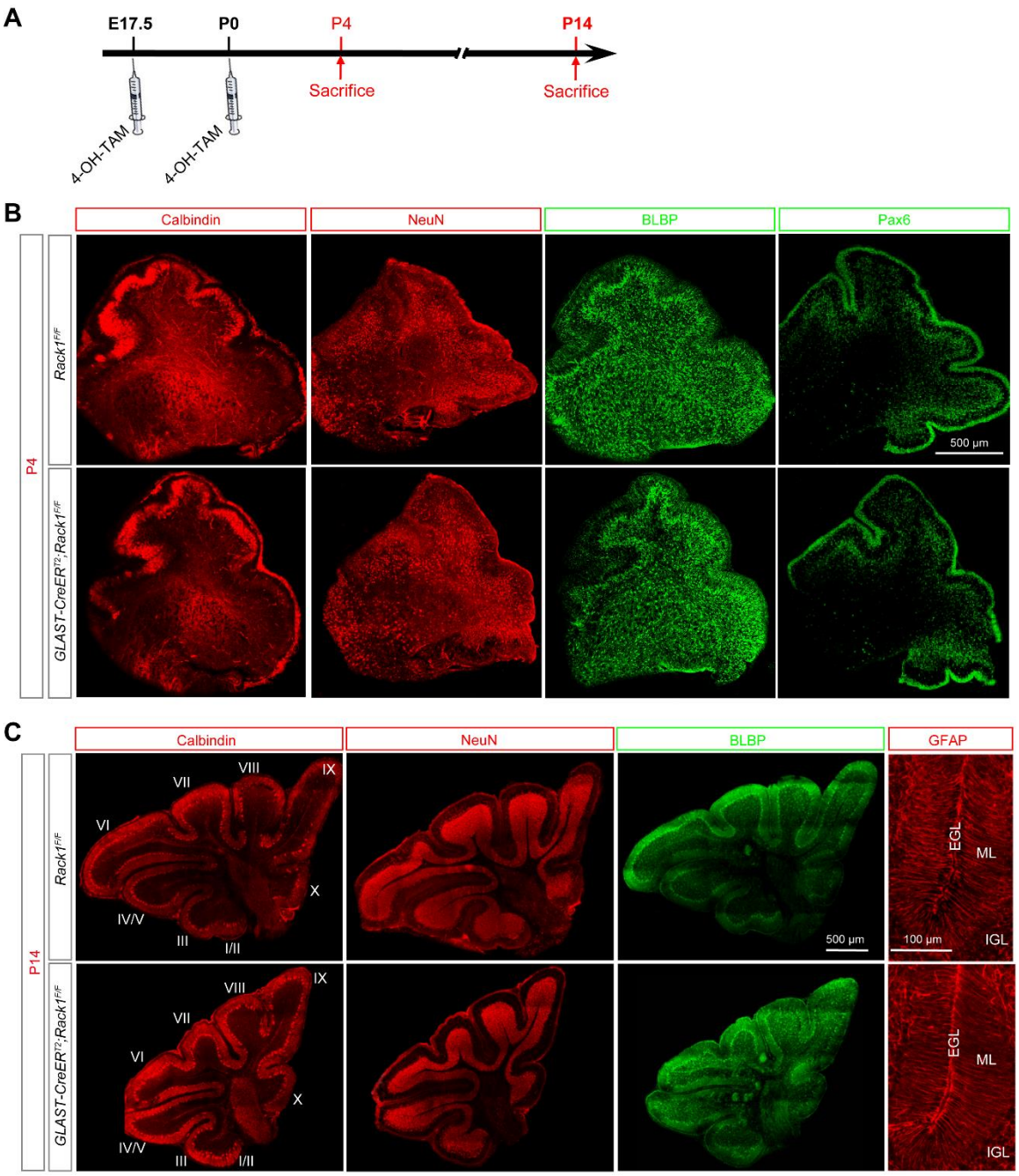

Fig. S8. Ablation of *Rack1* in BGs shows normal cerebellar morphogenesis. (A) A schematic showing the experimental design to *GLAST-CreER^{T2};Rack1$^{F/F}$* mutants. (B,C) Immunofluorescent staining of cerebellar sections in control and *GLAST-CreER^{T2};Rack1$^{F/F}$* mutants with anti-Calbindin, anti-NeuN, anti-BLBP and anti-Pax6 at

P4 and P14, respectively. Scale bar=500 μm. Enlarged images of the cerebellar lobules in control and *GLAST-CreER^{T2};Rack1$^{F/F}$* mutants are shown on the right. Scale bar=100 μm.

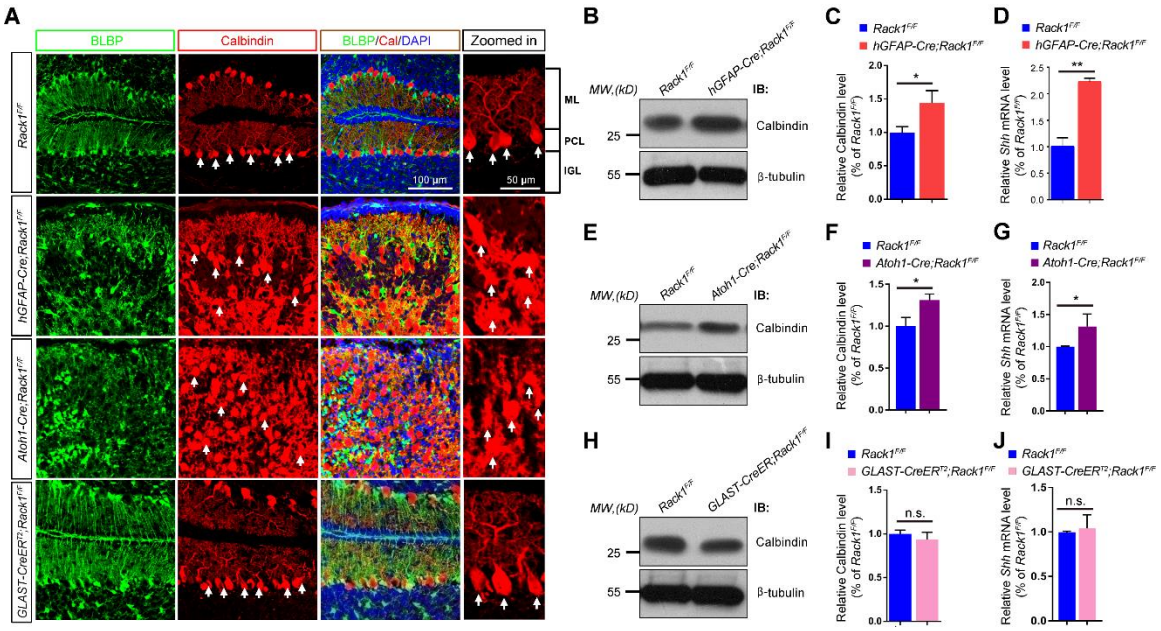

Fig. S9. Non cell-autonomous role of Rack1 in Purkinje cells. (A) Immunofluorescent staining of cerebellar sections with anti-BLBP and anti-Calbindin in indicated genotypes at P14. Arrows point to misaligned PCs with abnormal dendritic trees in *hGFAP-Cre;Rack1*$^{F/F}$ and *Atoh1-Cre;Rack1*$^{F/F}$ mutants but not in *Rack1*$^{F/F}$ control and *GLAST-CreER*^{T2}*;Rack1*$^{F/F}$ mutants. Scale bar=100 μm. Enlargement of t dendritic morphology of PCs are shown on the right. Scale bar=50 μm (B,C) Representative Western blot and quantification of Calbindin protein level in *Rack1*$^{F/F}$ control and *hGFAP-Cre;Rack1*$^{F/F}$ mutant cerebella. Mean±SEM; *P=0.0202, n=3. (D) mRNA expression of *Shh* in *Rack1*$^{F/F}$ control and *hGFAP-Cre;Rack1*$^{F/F}$ mutant cerebella was detected by quantitative real-time RT-PCR. Mean±SEM; **P<0.0001, n=3. (E,F) Representative Western blot and quantification of Calbindin protein level in *Rack1*$^{F/F}$ control and *Atoh1-Cre;Rack1*$^{F/F}$ mutant cerebella. Mean±SEM; *P=0.0132, n=3. (G) mRNA expression of *Shh* in *Rack1*$^{F/F}$ control and *Atoh1-Cre;Rack1*$^{F/F}$ mutant cerebellum was detected by quantitative real-time RT-PCR. Mean±SEM; *P=0.0465, n=3. (H,I) Representative Western blot and quantification of Calbindin protein level in *Rack1*$^{F/F}$ control and *GLAST-CreER*^{T2}*;Rack1*$^{F/F}$ mutant cerebella. Mean±SEM; P=0.3086, n=3. n.s., not significant. (J) mRNA expression of *Shh* in *Rack1*$^{F/F}$ control and *GLAST-CreER*^{T2}*;Rack1*$^{F/F}$ mutant

cerebella was detected by quantitative real-time RT-PCR. Mean±SEM; P=0.6674, n=3. n.s., not significant.

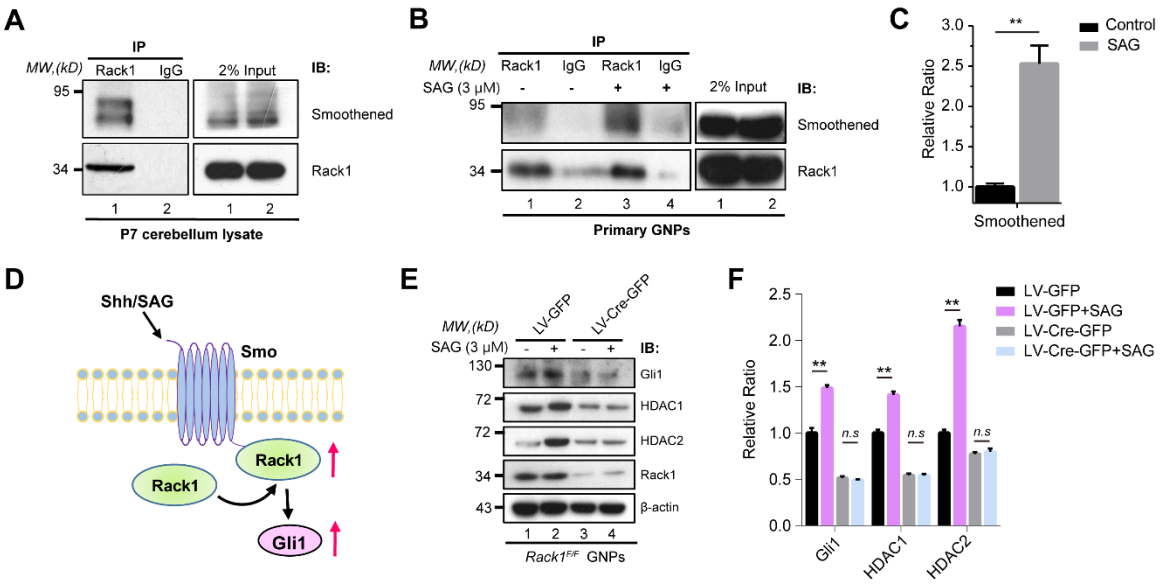

Fig. S10. Rack1 is essential for Shh signaling activation in primary GNPs by interacting with Smoothened and upregulating HDAC1/HDAC2 expression. (A) Co-immunoprecipitation demonstrate the interaction between Rack1 and Shh signaling receptor Smoothened in the cerebellum. P7 cerebellum lysate was incubated either with anti-Rack1 or control IgG. (B,C) Co-immunoprecipitation and quantification demonstrate the interaction between Rack1 and Smoothened was significantly enhanced in response to treatment with 3 μM Smoothened agnoist SAG. Mean±SEM; **P<0.0001, n=4. (D) A schematic model of Rack1 signaling. Rack1 is a critical mediator of Shh/SAG signaling that links activated Smoothened to upregulated downstream Gli1 expression. (E,F) Quantitative Western blot analysis indicates significantly increased expression of Gli1 and HDAC1/HDAC2 in response to 3 μM SAG treatment in control LV-GFP infected, but not LV-Cre-GFP infected *Rack1*$^{F/F}$ GNPs. Ablation of Rack1 expression in LV-Cre-GFP infected *Rack1*$^{F/F}$ GNPs was further confirmed by immunoblotting with anti-Rack1. Mean±SEM; **P=0.0002, 0.0001 and 0.0001, respectively, n=4.

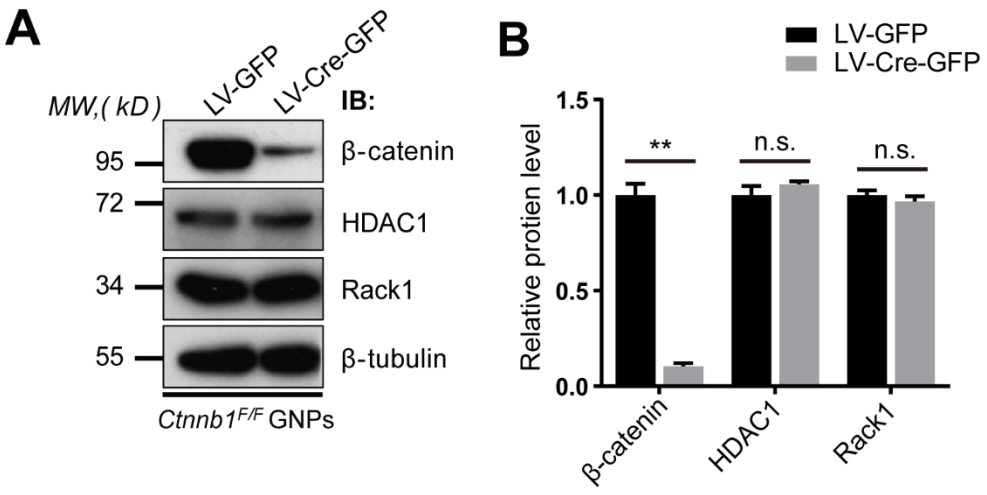

Fig. S11. Ablation of β-catenin in GNPs does not alter HDAC1 and Rack1 expression. (A) Representative Western blots examining the expression of β-catenin, HDAC1 and Rack1 in primary *Ctnnb1*$^{F/F}$ GNPs after infection with LV-Cre-GFP or LV-GFP control virus. (B) Quantitative analysis of Western blot results indicates a significant reduction of β-catenin (**P<0.0001), but the expression of HDAC1 and Rack1 are indistinguishable between LV-Cre-GFP and LV-GFP control infected cells. n.s., not significant. Mean±SEM; P=0.1301 and 0.2038, respectively, n=3.

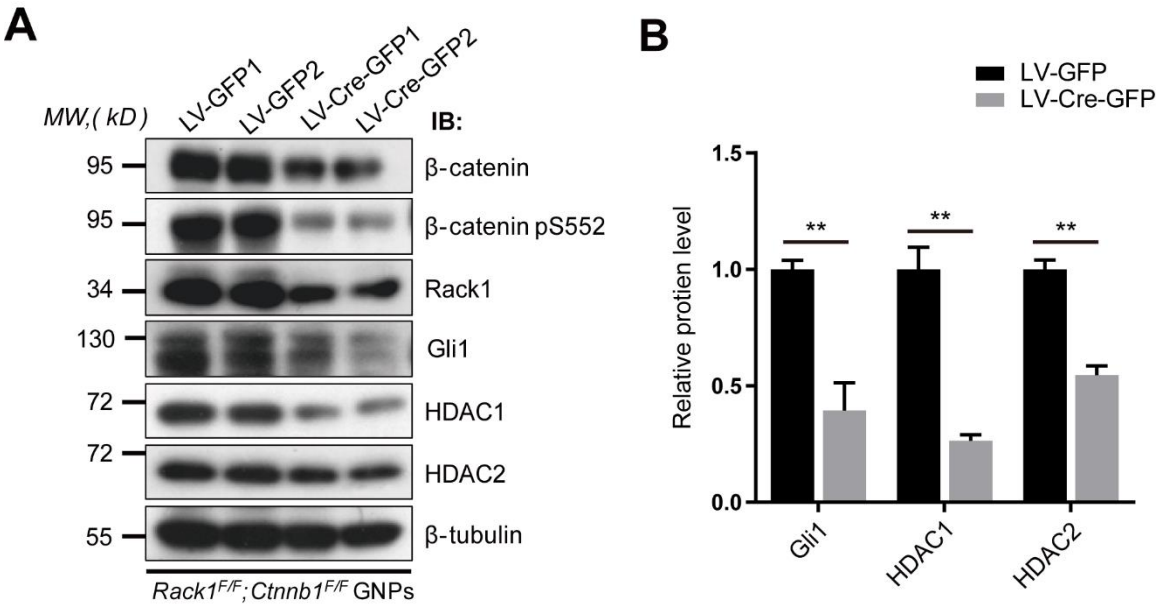

Fig. S12. Simultaneous deletion of β-catenin and Rack1 in GNPs does not alter Gli1 and HDAC1/HDAC2 expression. (A) Representative Western blots examining the expression of total β-catenin, active β-catenin (pS552), Rack1, Gli1 and HDAC1/HDAC2 in double-floxed *Rack1$^{F/F}$;Ctnnb1$^{F/F}$* GNPs after LV-GFP control or LV-Cre-GFP infection. (B) Quantitative analysis of Western blot results indicates significantly reduced Gli1, HDAC1 and HDAC2 in LV-Cre-GFP infected *Rack1$^{F/F}$;Ctnnb1$^{F/F}$* GNPs compared to LV-GFP-infected control. Mean±SEM; **P=0.0011, 0.0002 and 0.0002, respectively, n=3.

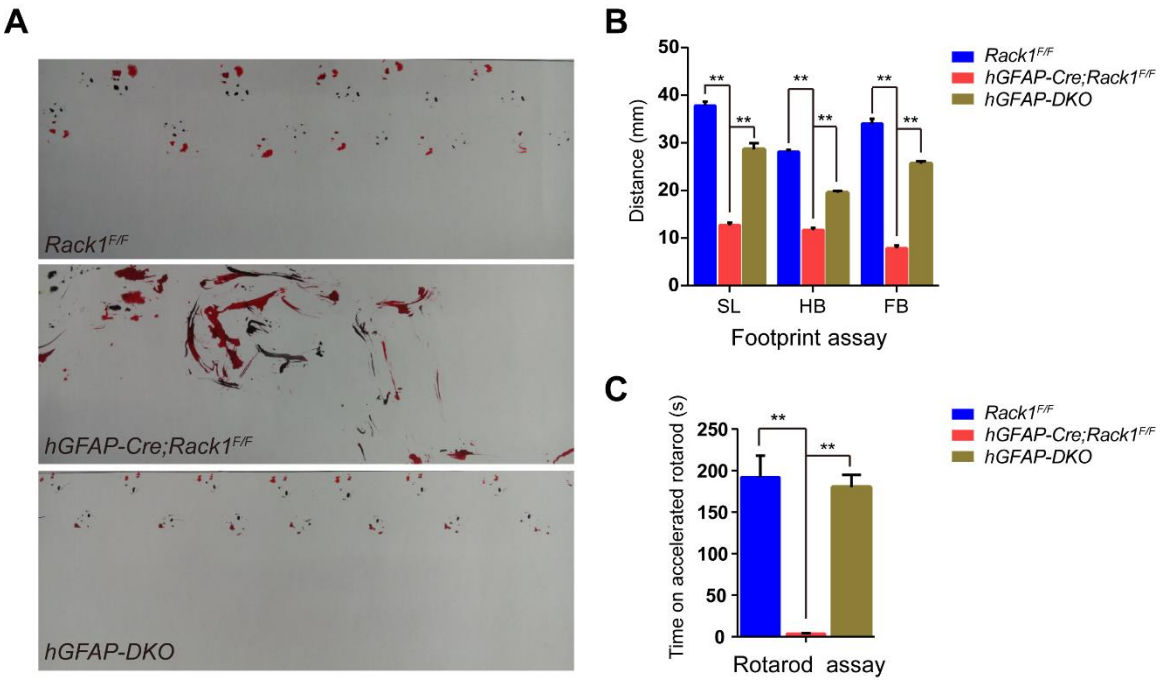

Fig. S13. Simultaneous deletion of β-catenin in *hGFAP-Cre;Rack1$^{F/F}$* mutants significantly rescues llocomotor defects. (A) Representative footprint patterns from P20 control, *hGFAP-Cre;Rack1$^{F/F}$* and *hGFAP-DKO* mutant mice. (B) Quantitation of walking patterns using distance shows impaired stride length (SL), hind-base width (HB) and fore-base width (FB) in *hGFAP-Cre;Rack1$^{F/F}$* mutant mice compared to *Rack1$^{F/F}$* controls, but significantly improved performance in *hGFAP-DKO* mutants. Mean±SEM; **P<0.0001, n≥6. (C) Quantitation of time spent on the accelerating rotarod in indicated genotypes. Mean±SEM; **P<0.0001, n≥6.

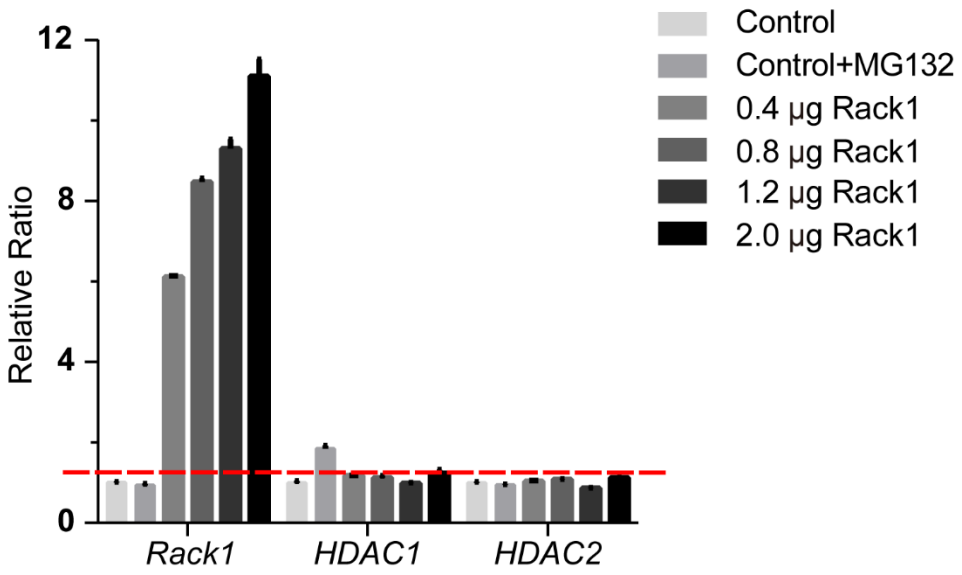

Fig. S14. Overexpression of Rack1 does not affect the HDAC1/HDAC2 transcription. HEK293 cells were treated with 20 μg/ml MG132, or transfected with indicated doses of an exogenous *Flag-Rack1* vector. The transcriptional level of endogenous *HDAC1/HDAC2* was detected by quantitative real-time RT-PCR. No significant difference in transcription was detected for both *HDAC1* and *HDAC2* after *Flag-Rack1* overexpression at indicated dosage. Mean±SEM. P>0.05, n=3.

Fig. S15. Uncropped Western blot images **1/10**

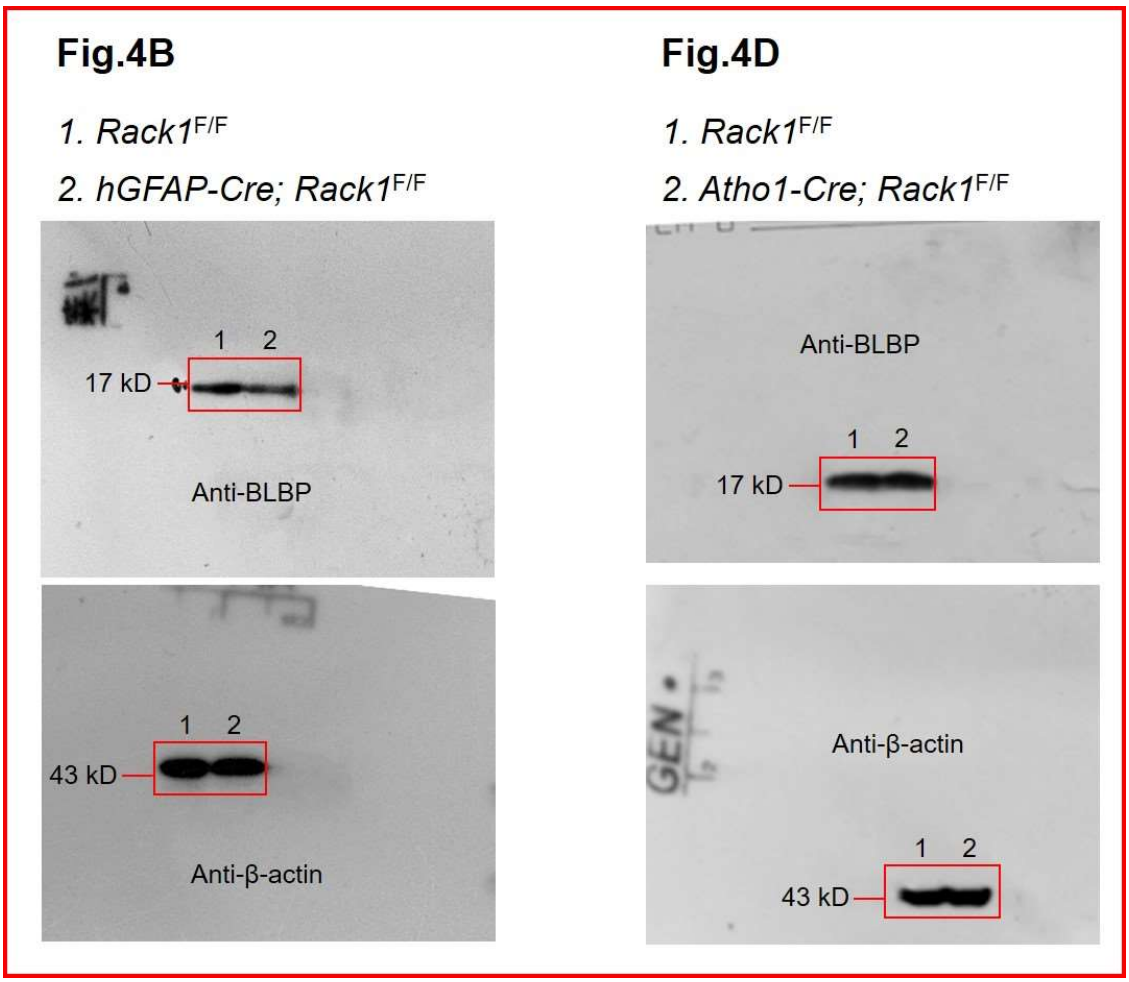

Fig. S15. Uncropped Western blot images **2/10**

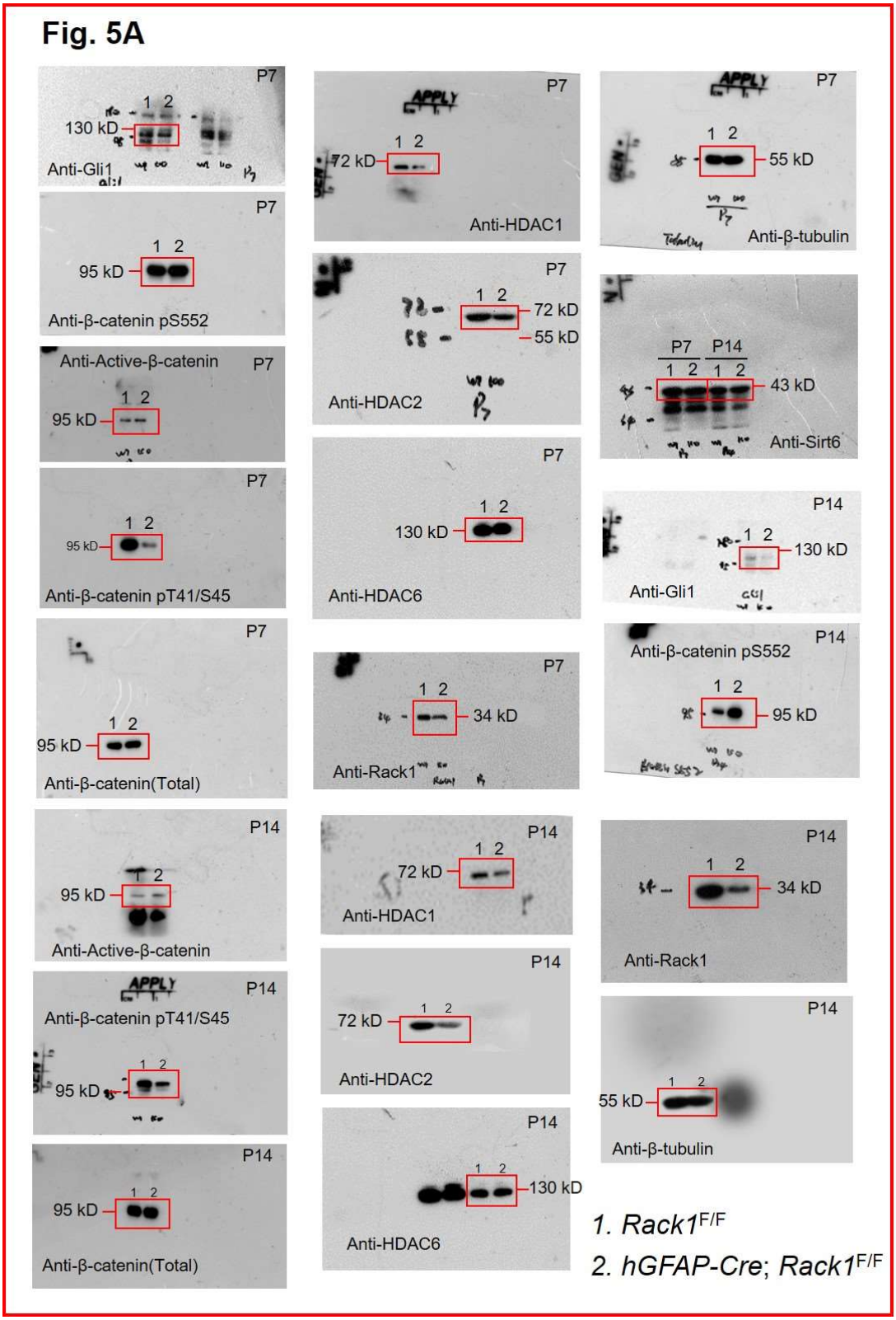

Fig. S15. Uncropped Western blot images **3/10**

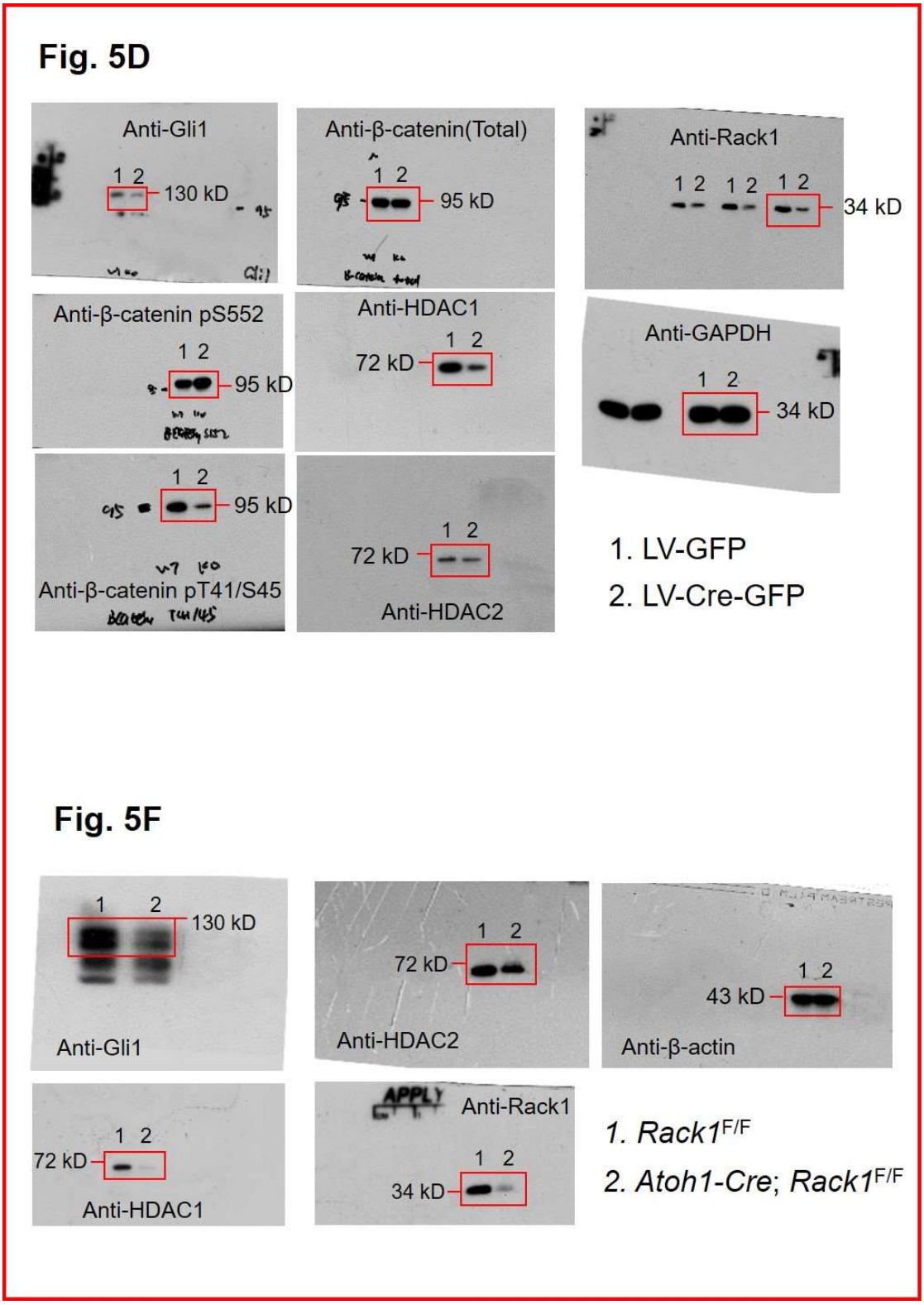

Fig. S15. Uncropped Western blot images **4/10**

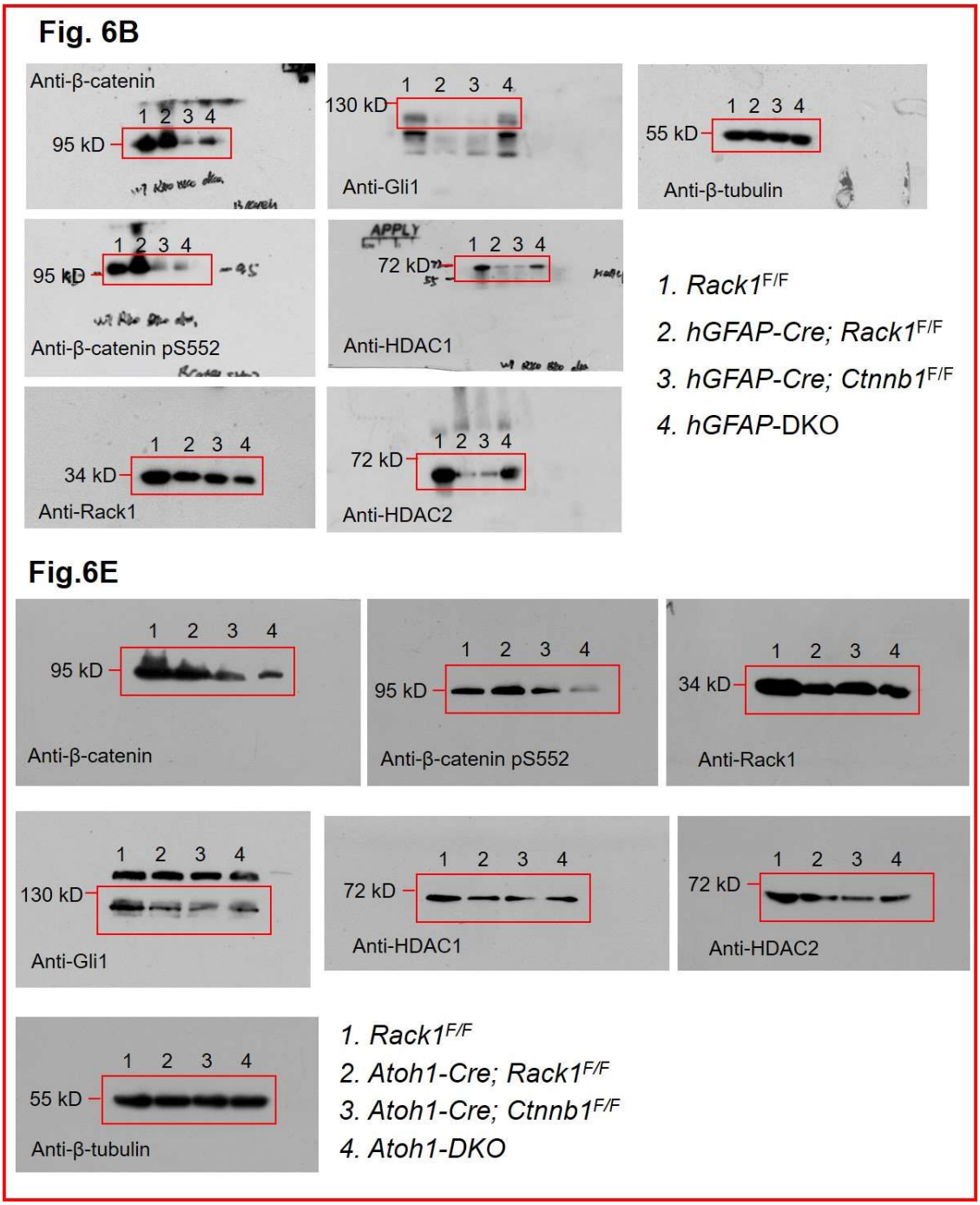

Fig. S15. Uncropped Western blot images 5/10

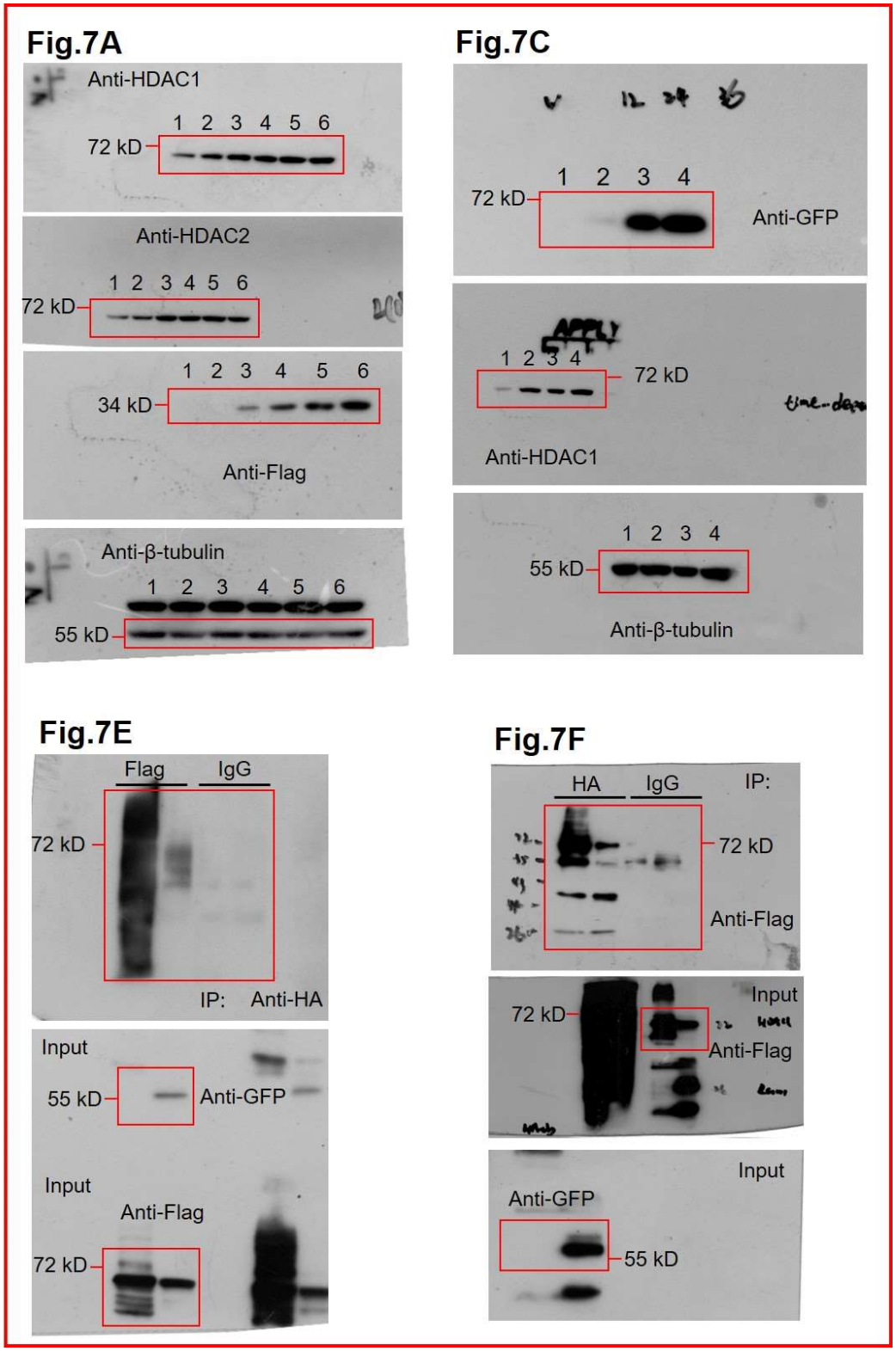

Fig. S15. Uncropped Western blot images **6/10**

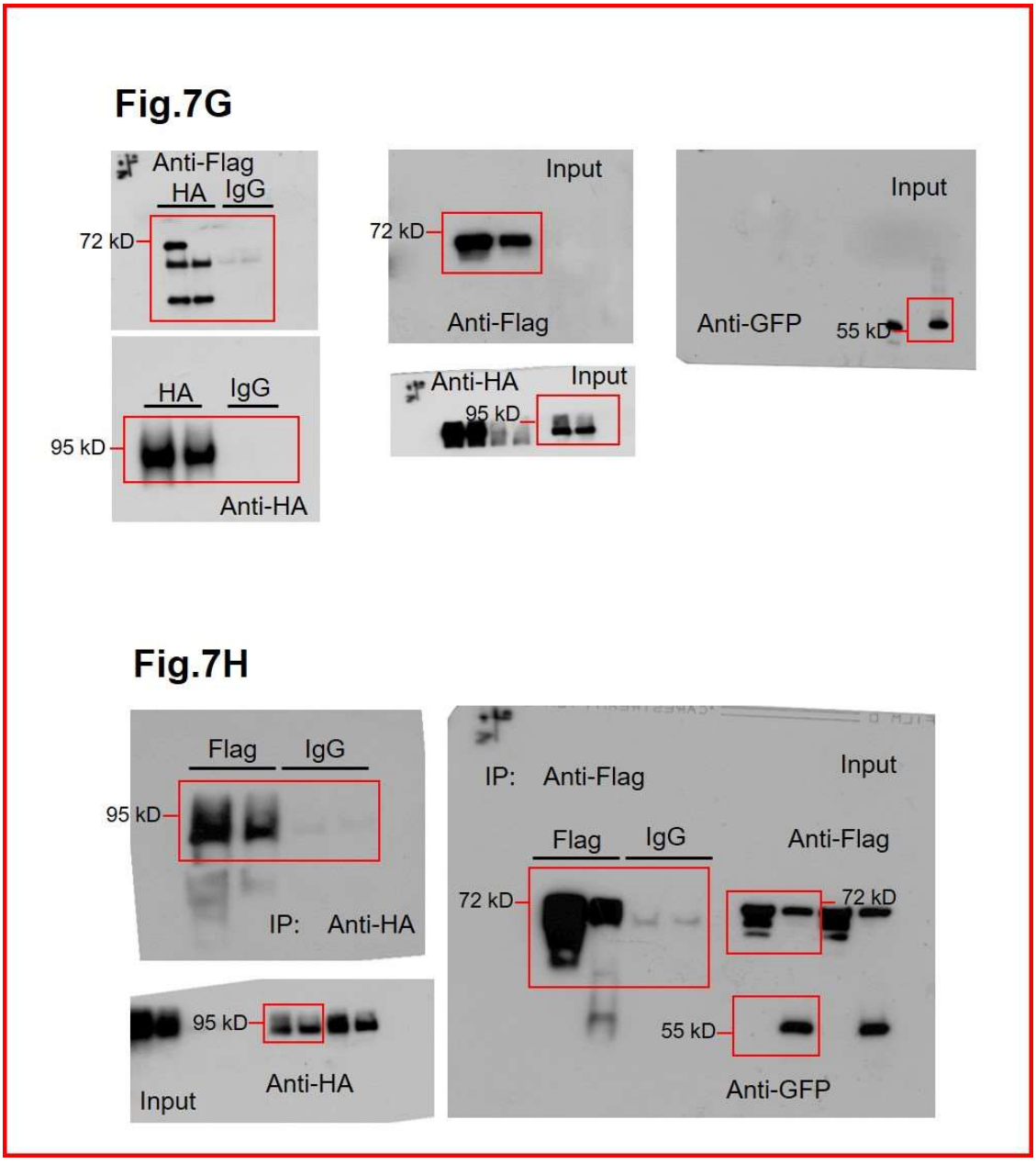

Fig. S15. Uncropped Western blot images 7/10

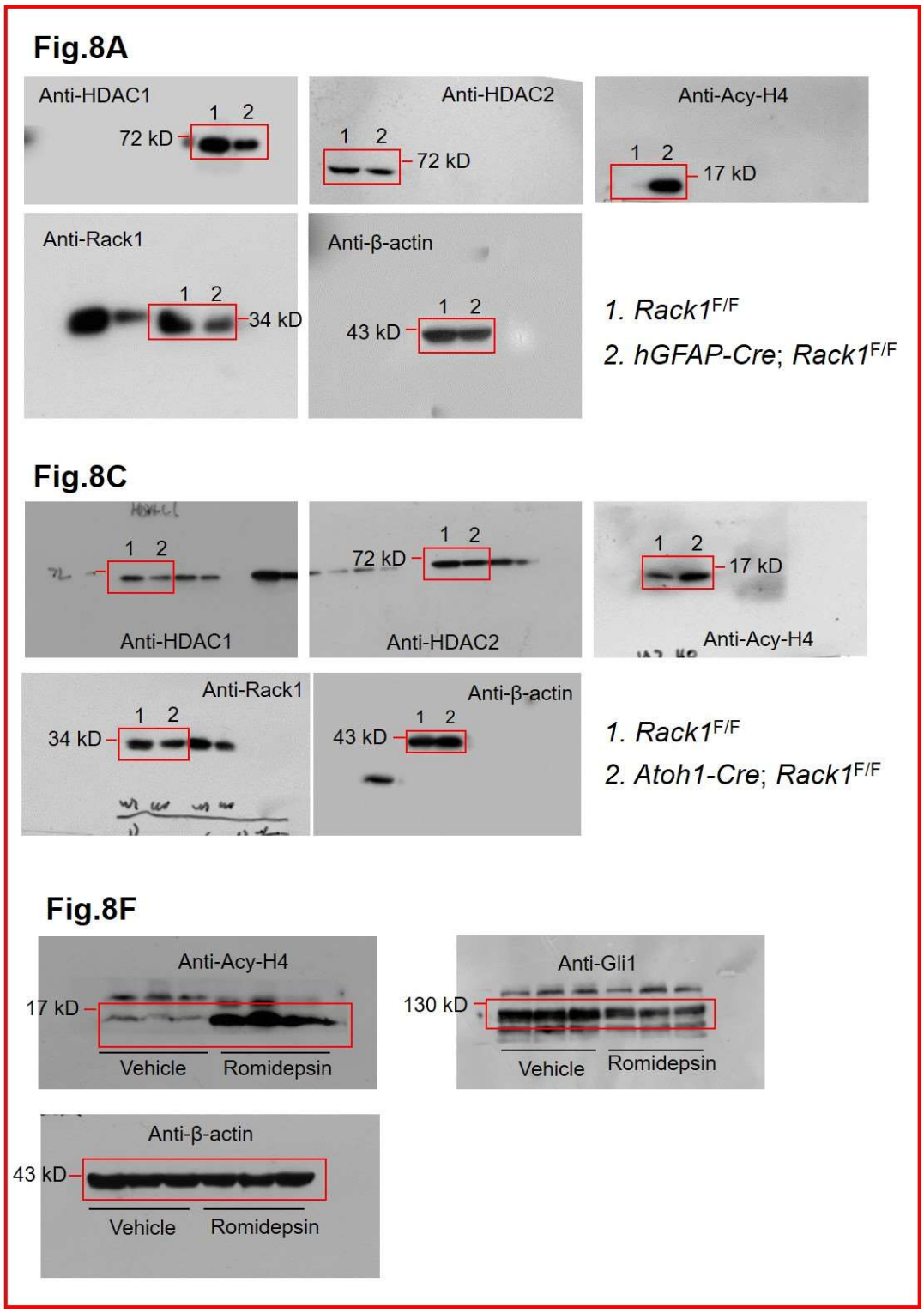

Fig. S15. Uncropped Western blot images **8/10**

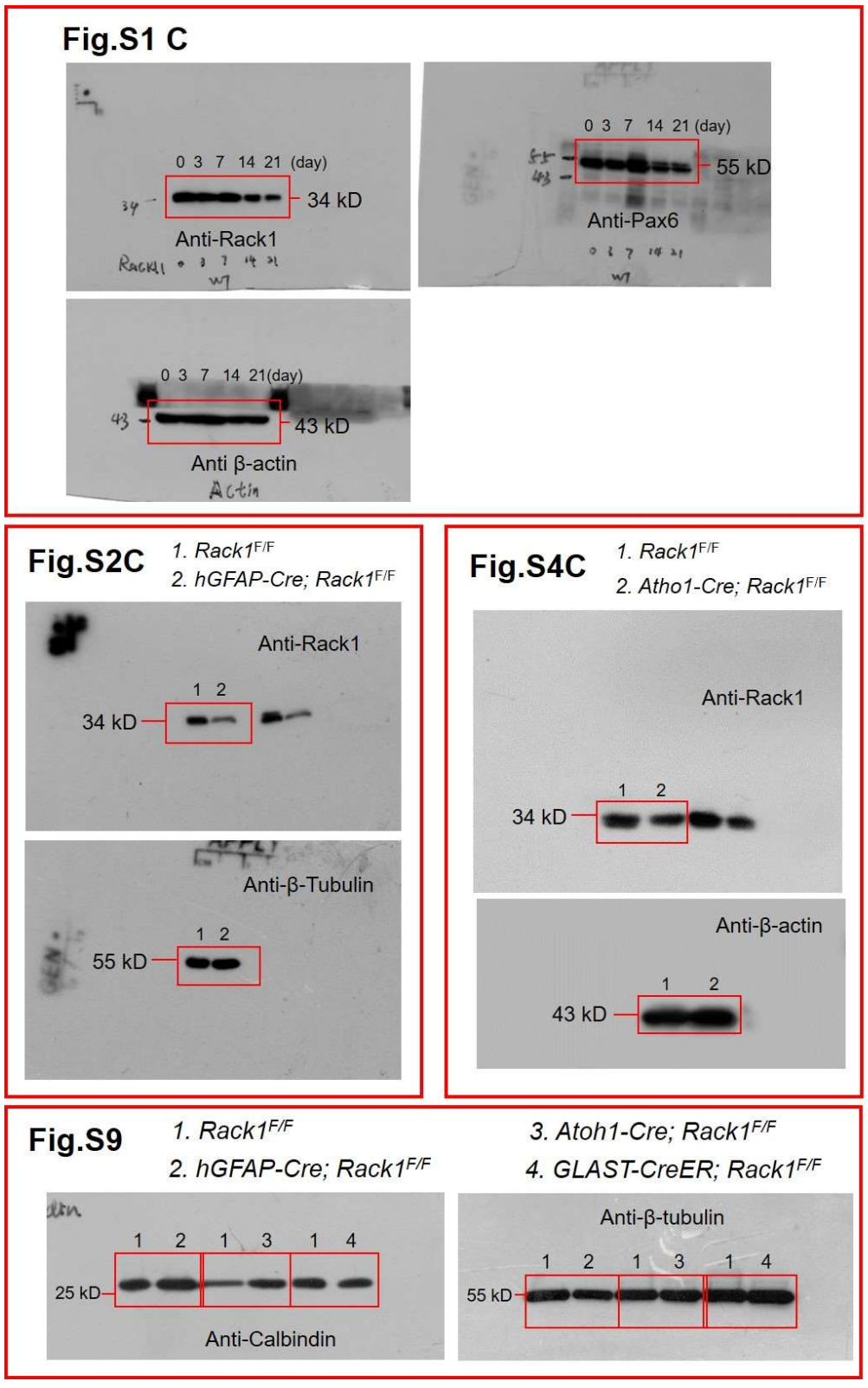

Fig. S15. Uncropped Western blot images 9/10

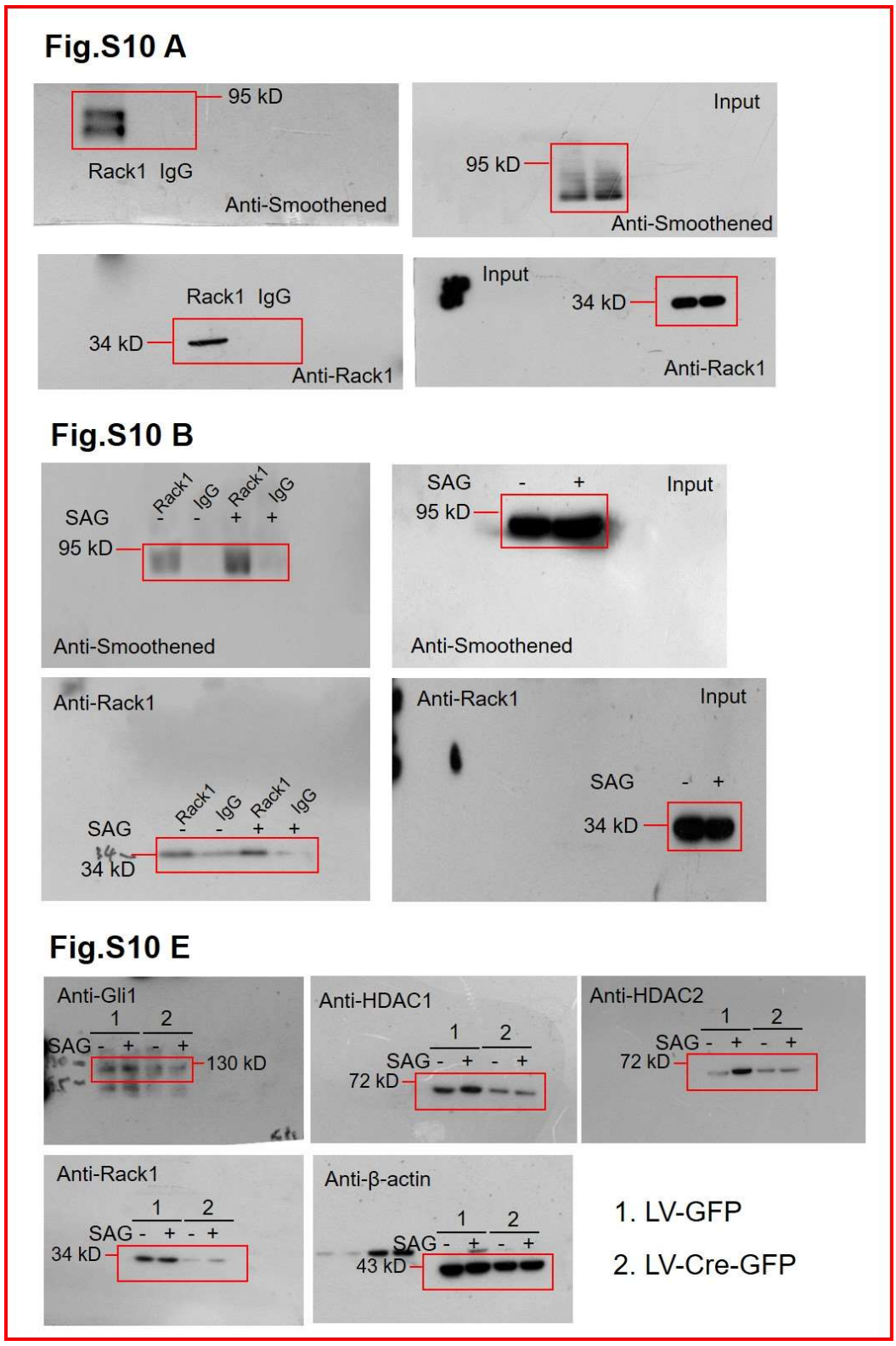

Fig. S15. Uncropped Western blot images **10/10**

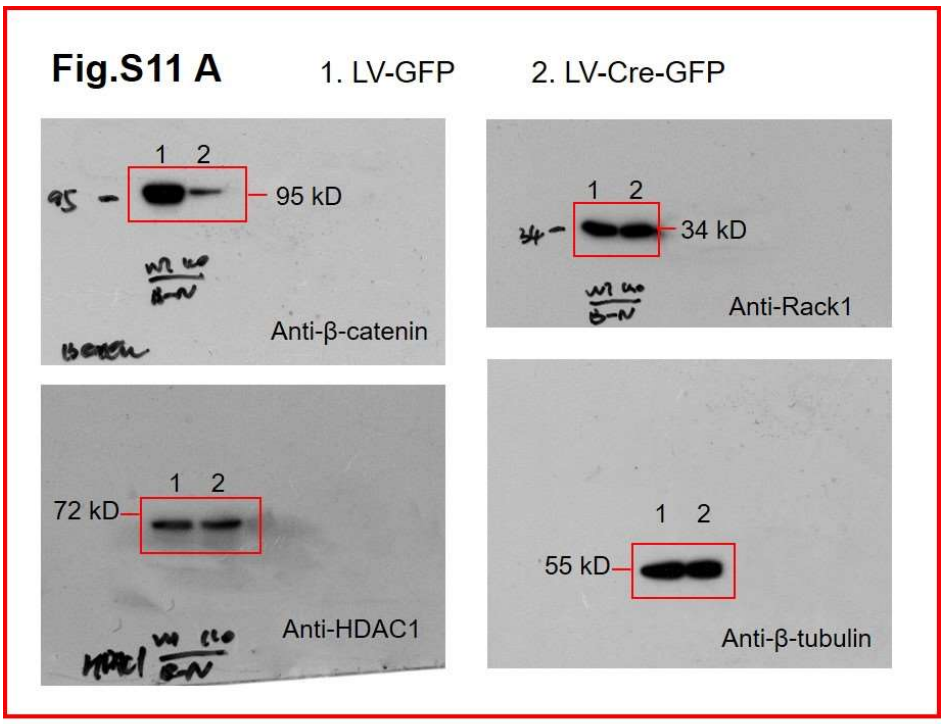

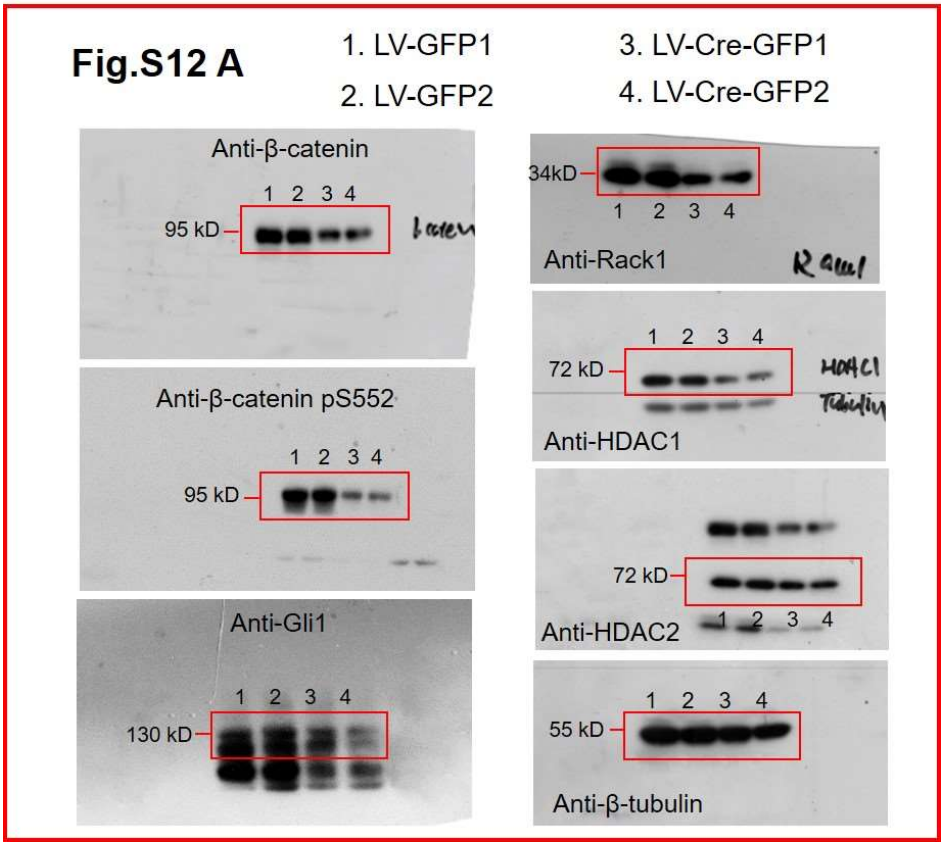

Table S1. Mouse-specific primers used for qRT-PCR

Primers	Forward	Reverse
GAPDH	AGGTCGGTGTGAACGGATTTG	TGTAGACCATGTAGTTGAGGTCA
HDAC1	AGTCTGTTACTACTACGACGGG	TGAGCAGCAAATTGTGAGTCAT
HDAC2	GGAGGAGGCTACACAATCCG	TCTGGAGTGTTCTGGTTTGTCA
P21	CCTGGTGATGTCCGACCTG	CCATGAGCGCATCGCAATC
MycN	CGGTGAACAAGCGAGAGTC	GGGGCAGTAGCTGGAACAG
Ptch1	AAAGAACTGCGGCAAGTTTTTG	CTTCTCCTATCTTCTGACGGGT
Gli1	CCAAGCCAACTTTATGTCAGGG	AGCCCGCTTCTTTGTTAATTTGA
Gli2	CAACGCCTACTCTCCCAGAC	GAGCCTTGATGTACTGTACCAC
Gli3	CACAGCTCTACGGCGACTG	CTGCATAGTGATTGCGTTTCTTC
Cyclin D1	GCGTACCCTGACACCAATCTC	CTCCTCTTCGCACTTCTGCTC
LEF1	TGTTTATCCCATCACGGGTGG	CATGGAAGTGTCGCCTGACAG
TCF1	CGAGATGCTATCTTCAAGCAGTT	GTACACGTTAAACCACTCGGG
Axin2	TGACTCTCCTTCCAGATCCCA	TGCCCACACTAGGCTGACA
Pax6	TACCAGTGTCTACCAGCCAAT	TGCACGAGTATGAGGAGGTCT
TAG1	TGTCTGTGCGAGATGCAAC	CCATAGTGGGGTCATGCGAG
ZIC1	CAGTATCCCGCGATTGGTGT	GCGAACTGGGGTTGAGCTT
Atoh1	GAGTGGGCTGAGGTAAAAGAGT	GGTCGGTGCTATCCAGGAG
Reelin	TTACTCGCACCTTGCTGAAAT	CAGTTGCTGGTAGGAGTCAAAG
Rack1	ACTCCCACTTCGTTAGTGATGT	CCCGTTGTGAGATCCCAGAG

References

1. Ashique AM*, et al.* (2006) Localization of the scaffolding protein RACK1 in the developing and adult mouse brain. *Brain Res* 1069(1):31-38.
2. Zhuo L*, et al.* (2001) hGFAP-cre transgenic mice for manipulation of glial and neuronal function in vivo. *Genesis* 31(2):85-94.
3. Sanchez-Ortiz E*, et al.* (2014) NF1 regulation of RAS/ERK signaling is required for appropriate granule neuron progenitor expansion and migration in cerebellar development. *Genes Dev* 28(21):2407-2420.
4. Zhao Y*, et al.* (2015) RACK1 Promotes Autophagy by Enhancing the Atg14L-Beclin 1-Vps34-Vps15 Complex Formation upon Phosphorylation by AMPK. *Cell Rep* 13(7):1407-1417.
5. Ben-Arie N*, et al.* (1997) Math1 is essential for genesis of cerebellar granule neurons. *Nature* 390(6656):169-172.
6. Ben-Arie N*, et al.* (2000) Functional conservation of atonal and Math1 in the CNS and PNS. *Development* 127(5):1039-1048.
7. Machold R & Fishell G (2005) Math1 is expressed in temporally discrete pools of cerebellar rhombic-lip neural progenitors. *Neuron* 48(1):17-24.
8. Wang VY, Rose MF, & Zoghbi HY (2005) Math1 expression redefines the rhombic lip derivatives and reveals novel lineages within the brainstem and cerebellum. *Neuron* 48(1):31-43.
9. DeBoer EM & Rasin MR (2013) Nucleoside analog labeling of neural stem cells and their progeny. *Methods Mol Biol* 1018:21-37.
10. Insolera R, Bazzi H, Shao W, Anderson KV, & Shi SH (2014) Cortical neurogenesis in the absence of centrioles. *Nat Neurosci* 17(11):1528-1535.
11. Schuller U & Rowitch DH (2007) Beta-catenin function is required for cerebellar morphogenesis. *Brain Res* 1140:161-169.
12. Wen J, Yang HB, Zhou B, Lou HF, & Duan S (2013) beta-Catenin is critical for cerebellar foliation and lamination. *PLoS One* 8(5):e64451.
13. Lorenz A*, et al.* (2011) Severe alterations of cerebellar cortical development after constitutive activation of Wnt signaling in granule neuron precursors. *Mol Cell Biol* 31(16):3326-3338.
14. Lee HY, Greene LA, Mason CA, & Manzini MC (2009) Isolation and culture of post-natal mouse cerebellar granule neuron progenitor cells and neurons. *Journal of visualized experiments : JoVE* (23).
15. Romer JT*, et al.* (2004) Suppression of the Shh pathway using a small molecule inhibitor eliminates medulloblastoma in Ptc1(+/-)p53(-/-) mice. *Cancer Cell* 6(3):229-240.
16. Kim JY, Grunke SD, Levites Y, Golde TE, & Jankowsky JL (2014) Intracerebroventricular viral injection of the neonatal mouse brain for persistent and widespread neuronal transduction. *J Vis Exp* (91):51863.